NOVEL METHODS FOR WEAK PHYSIOLOGICAL PARAMETERS MONITORING

A THESIS SUBMITTED TO THE GRADUATE DIVISION OF THE UNIVERSITY OF HAWAIʻI AT MĀNOA IN PARTIAL FULFILLMENT OF THE REQUIREMENTS FOR THE DEGREE OF

MASTER OF SCIENCE

IN

ELECTRICAL ENGINEERING

MAY 2017

By

Jia Xu

Thesis Committee:

Olga Boric-Lubecke, Chairperson
Victor M. Lubecke
Anthony Kuh

Keywords: Physiological monitoring, bio-impedance analysis, Doppler radar

Dedication

to my parents –
Jian Xu and Hua Zhou

Acknowledgement

First and foremost, I would like to sincerely thank my advisor, Prof. Olga Boric-Lubecke, for her tremendous supports of my master study and research, for her guidance and consistent encouragement. I am very grateful for all the opportunities she provided me, which greatly enriched my experience and life.

I also thank the rest of my thesis committee, Prof. Victor Lubecke and Prof. Anthony Kuh, for their insightful comments and valuable discussions, which incented me to widen my research from various perspectives.

My sincere thank also goes to my lab colleagues, Ehsan Yavari, Ashikur Rahman, Shuhei Yamada, and Alex Lee, for their friendship and assistance on the research.

I would like to express my special appreciation to my fiancé, Xiaomeng Gao, who introduced me to this excellent group and opened the door of this wonderful journey. He has always been patient, encouraging, and supportive over the past two years, which helped to keep me being positive and brave to get through all the difficulties.

Last but not least, I would like to dedicate my sincerest gratitude and love to my parents, Jian Xu and Hua zhou, whose selfless love and endless caring made me who I am today. This work would not be possible without their support and encouragement.

Abstract

Physiological monitoring systems that monitor vital sign parameters associated with physiological activities are important for health condition prognosis and diagnosis. These systems use transducers to detect weak physiological parameters, such as electrical signals (potential, impedance, capacitance) and mechanical variations (displacement), for interpretation of vital signs. Continuous heart rate monitoring is one of the most important practices by physicians. It assesses the cardiovascular condition of a subject and is normally carried out on special medical devices by personnel with specified training in hospitals, such as 12-lead electrocardiogram (ECG). Though it provides reliable readings of heartbeat signal, the wiring configurations may interfere cardiovascular activity pattern as well as refrain subject's daily activities. And it is hard to be used in non-clinical environment without the help of professional personnel.

In this work, a bio-impedance analysis (BIA) based contact method and Wi-Fi band Doppler radar based non-contact method are proposed. The BIA system was able to estimate heart rate from the subject's wrist with only four electrodes. The BIA results agree with the reference, which validates the feasibility of the proposed system. To the best of our knowledge, this is the first reported BIA heartbeat monitoring system in the wristband configuration. In addition, an assessment of a variety of conventional biosensors for vital sign sensing was conducted, which evaluated their capabilities of acquiring heart rate or respiration rate from non-conventional locations. The extensive data collected and analyzed provided in-depth understanding of each sensor's performance and potential application in wearable healthcare devices. The Doppler radar system was intended to detect small displacements on the body surface resulting from cardiac activities. Such time dependent variations indicate the impact of the heartbeat on the surface of chest wall, thus applicable for heart rate extraction. The lead-free feature of radar sensor eliminates any wiring configuration to the subject, and is a good candidate of non-contact physiological monitoring.

Table of Contents

Acknowledgement iii
Abstract iv
Table of Contents v
List of Tables vii
List of Figures viii
List of Abbreviations and Symbols x
Chapter 1. Introduction 1
1.1 Overview 1
1.2 Contribution 2
1.3 Thesis organization 3
Chapter 2. Literature Review 5
2.1. Contact sensing 5
2.2. Radar-based non-contact sensing 8
2.2.1. Non-contact physiological sensing 8
2.2.2. Physiological parameter extraction 9
2.3. Summary 10
Chapter 3. Bio-impedance Based Physiological Monitoring 11
3.1. Introduction to Bio-impedance Analysis 11
3.2. Heartbeat measurement principle based on BIA 12
3.3. Measurement system design 14
3.4. Experiment set-up 16
3.5. Human testing results and discussions 18
3.6. Summary 20
Chapter 4. Comparison of Contact Sensors 21
4.1. Measurement overview 21
4.2. Sensor measurement for heart rate and respiratory rate 22

4.2.1. Electrocardiogram (ECG) 22
4.2.2. Infrared wrist watch 25
4.2.3. Bio-impedance analyzer (BIA) 33
4.3. Summary 40
Chapter 5. Continuous-wave Radar for Physiological Monitoring 42
5.1. Doppler radar measurement system 42
5.1.1. Measurement Principle 42
5.1.2. Doppler Radar Fundamentals 43
5.1.3. Summary 51
5.2. Doppler Radar Sub-Millimeter Physiological Displacement Estimation 52
5.2.1. Experiment set-up 52
5.2.2. Measurement results and discussions 54
5.2.3. Summary 60
Chapter 6. Conclusion 61
6.1. Challenges 61
6.2. Summary 61
6.3. Future work 62
Appendix A. Bio-impedance Analysis Human Testing Protocol 64
A.1. CHS #19176 Research Protocol 64
1. Specific Aims 64
2. Background and Significance 65
3. Preliminary Studies 66
4. Research Design and Methods 66
5. Experimental Methods: 66
6. Data and Safety Monitoring Plan 69
7. Literature Cited 69
A.2. CHS #19176 Consent Form 71
A.3. CHS #19176 Approval Letter 78
References 79

List of Tables

Table 3.1 Heart Rate Experiment Results 20
Table 4.1 Summary on biosensors, instrumentations and accessories 21
Table 4.2 Heart rate measurement for ECG over chest and finger pulse transducer 24
Table 4.3 Heart rate and respiratory rate detectable location summary 40
Table 5.1 Comparison of displacement measurement results 55
Table A.1 The experiments consist of the following equipment 68

List of Figures

Figure 2.1 3-lead ECG configuration 5
Figure 2.2 (a) A demonstration of sensor with piezoelectric effect. (b) Samples of piezoelectric pieces 6
Figure 2.3 Transmissive and reflective ways 7
Figure 3.1 (a) Electrical model of blood cells. (b) Flow paths of alternative current with different frequencies. 11
Figure 3.2 4-elecrode configuration. 12
Figure 3.3 Electrical impedance model for blood including impedance variation related to heartbeat [73]. 13
Figure 3.4 Wrist model and tetra-polar configuration for bio-impedance sensing, where red dots represent driving electrodes and black ones represent sensing electrodes [74]. 14
Figure 3.5 Block diagram of heart-related impedance variation measurement. 15
Figure 3.6 Settings of electrodes 17
Figure 3.7 Experiment results of subject #1 from lower wrist (a) (b) (c) 19
Figure 4.1 Reference sensors (a) Piezoelectric pulse transducer, (b) inductive plethysmography belt, (c) piezoelectric chest belt 22
Figure 4.2 Electrode positions of ECG testing. (a) chest front, (b) chest left side, (c) chest back, (d) upper arm 23
Figure 4.3 Time domain ECG measurement results in comparison with finger pulse sensor results. (a) chest front, (b) chest left side, (c) chest back, (d) upper arm. 24
Figure 4.4 Frequency domain ECG measurement result of upper arm in comparison with finger pulse sensor. 25
Figure 4.5 (a) Back view of the AFE4403 watch showing the infrared sensor. (b) Right-side view of the watch showing microUSB connector. 26
Figure 4.6 Testing locations for IR watch. (a) chest front, (b) chest left side, (c) chest back, (d) upper arm, (e) lower wrist, (f) upper wrist. 26
Figure 4.7 Upper wrist measurement results with IR watch. (a) heart rate in frequency domain (b) respiratory rate in time domain. 28
Figure 4.8 Lower wrist measurement results with IR watch. (a) heart rate in frequency domain (b) respiratory rate in time domain. 29
Figure 4.9 Upper arm measurement results with IR watch. (a) heart rate in frequency domain (b) respiratory rate in time domain 30
Figure 4.10 Front chest measurement results with IR watch. (a) heart rate in frequency domain (b) respiratory rate in time domain. 31
Figure 4.11 Side chest measurement results with IR watch. (a) heart rate in frequency domain (b) respiratory rate in time domain. 32

Figure 4.12 Back chest measurement results with IR watch. (a) heart rate in frequency domain (b) respiratory rate in time domain. 33
Figure 4.13 Tetrapolar configurations of bio-impedance analyzer for respiration and heartbeat measurement. (a) wrist lower, (b) upper arm, (c) chest front, (d) chest side, (e) chest back. 34
Figure 4.14 Lower wrist measurement results with BIA. (a) heart rate in frequency domain (b) respiratory rate in time domain. 35
Figure 4.15 Upper arm measurement results with BIA. (a) heart rate in frequency domain (b) respiratory rate in time domain. 36
Figure 4.16 Front chest measurement results with BIA. (a) heart rate in frequency domain (b) respiratory rate in time domain. 37
Figure 4.17 Side chest measurement results with BIA. (a) heart rate in frequency domain (b) respiratory rate in time domain. 38
Figure 4.18 Back chest measurement results with BIA. (a) heart rate in frequency domain (b) respiratory rate in time domain. 39
Figure 5.1 Architecture of CW Quadrature Doppler radar 44
Figure 5.2 Complex plane demonstration of I/Q channel baseband signal transcribing an arc (AB represents baseband signal amplitude) 48
Figure 5.3 Arc with dc offset 49
Figure 5.4 Finding arc radius 50
Figure 5.5 Long arc and short arc sharing the same radius 51
Figure 5.6 Linear stage displacement measurement 52
Figure 5.7 Experimental set-up configuration of quadrature Doppler radar, ARTrack infrared camera system, and linear stage. 54
Figure 5.8 Measured displacement comparison 56
Figure 5.9 Standard deviation comparison 57
Figure 5.10 Absolute error comparison 57
Figure 5.11 Relative error comparison 58
Figure 5.12 Time domain comparison of (a) 1.0mm displacement and (b) 0.3mm displacement estimations with reference. Dotted line is computer simulation of standard sinusoid with same displacement and 1Hz frequency, which represents the output of linear stage. Solid line is the reconstructed displacement measured by radar. Dash line stands for camera results. 59

List of Abbreviations and Symbols

Abbreviations

A/D	Analog-to-Digital Converter
AC	Alternate Current
AD	Arctangent Demodulation
ARTrack	Advanced Realtime Tracking
BIA	Bio-impedance Analysis
BMI	Body Mass Index
BOC	Board of Certification
BPM	Beats Per Minute
CFR	Code of Federal Regulations
CHS	Committee on Human Studies
CSD	Complex Signal Demodulation
CW	Continuous Wave
DAQ	Data Acquisition
DC	Direct Current
EC	Extracellular
ECG	Electrocardiogram
EMG	Electromyogram
FCC	Federal Communications Commission
FIR	Finite Impulse Response
FMCW	Frequency-modulated CW
HRV	Heart Rate Variability
IA	Instrumentation Amplifier
IC	Intracellular
ICA	Independent Component Analysis

IF	Intermediate Frequency
I/Q	In-phase/Quadrature-phase
IR	Infrared
IRB	Institution Review Board
LED	Light-emitting Diode
LNA	Low-noise Amplifier
LO	Local Oscillator
LVDT	Liner Variable Differential Transformer
PCB	Printed Circuit Board
PD	Photodetector
PI	Principle Investigator
PPG	Photoplethysmography
PTT	Pulse Transit Time
PWV	Pulse Wave Velocity
RA	Research Assistant
RER	Respiratory Exchange Ratio
RF	Radio-frequency
RSA	Respiratory Sinus Arrhythmia
RX	Receiving
SIDS	Sudden Infant Death Syndrome
TX	Transmitting
UWB	Ultra-wide Band
UH	University of Hawaii

Symbols

R_i	Resistance of the inner part of the blood cell (Ω)
R_e	Resistance of the extracellular medium (Ω)
C_m	Cell membrane capacitance (F)
Z_0	Constant impedance of wrist tissues (Ω)
$\Delta Z(t)$	Impedance variations directly related to heartbeat (Ω)
$V(t)$	A sinusoidal signal whose amplitude is modulated by the impedance variation resulted from heartbeat pulses (V)
R	Resistor (Ω)

G_1, G_2	Gains of the IA
f_d	Doppler frequency shift (rad)
f_t	Frequency of the transmitting signal (Hz)
v_r	Radial velocity of the moving target (m/s)
c	Speed of light (300,000km/s)
λ	Wavelength of carrier (m)
$\theta(t)$	Phase content or arc length transcribed by I/Q signals proportional to detected motion (rad)
$x(t)$	Object displacement variation (m)
f	Carrier frequency (Hz)
A_T	Amplitude of transmitting signal (V)
$\Phi(t)$	Phase noise of the oscillator in signal generator (rad)
ω	Angular frequency (rad)
d_0	Transmitted signal traveled distance (m)
$R(t)$	Backscattered signal (V)
θ_0	Constant phase shift (rad)
A_R	Backscattered signal amplitude (V)
$I(t)$	I channel signal (V)
$Q(t)$	Q channel signal (V)
$B_I(t)$	Baseband signal of interest
A_B	Baseband signal amplitude (V)
$\Delta\Phi(t)$	Residual phase noise (rad)
θ	Total constant phase shift due to the distance between target and radar (rad)
ϕ	Demodulated phase (rad)
$\tilde{\varphi}$	Demodulated phase after rotation (rad)
V_I	Constant dc offset in I channel (V)
V_Q	Constant dc offset in Q channel (V)

Chapter 1. Introduction

1.1 Overview

Physiological monitoring systems are commonly used in hospitals and care facilities for patient vital sign monitoring. The associated parameters can be used to assess the functionality of the physiological activities for health condition prognosis and diagnosis. The electrical or mechanical activities associated with the mechanism of human circulation, metabolism and respiration are often reflected by weak physiological parameters, such as heart rate, respiration rate, end-tidal CO2 level, blood oxygen saturation level, blood pressure, and etc. These parameters are vital indicators to the integrity of the human physical condition. Monitoring systems use transducers to detect such weak physiological parameters, such as electrical signals (potential, impedance, capacitance) and mechanical signals (displacement), for interpretation of vital signs.

Heartbeat signal is one of the most important indicators of heart problems. Monitoring heartbeat during everyday life not only could be helpful for early detection of heart disease, but also can help monitor the health status of subjects suffering from heart disease and patients in rehabilitation state. Heart disease (which includes Heart Disease, Stroke and other Cardiovascular Diseases) is the NO.1 cause of death in the United States. People with all ages and backgrounds can get the condition. According to the National Vital Statistics Reports, about 614,000 people were killed by diseases of the heart in 2014 [1]. Early detection of heart disease enables timely and more effective treatments, thus opening up the important possibilities of preventing late disease diagnosis or even fatal consequences. The rising need of everyday health care at home also makes heartbeat monitoring devices necessary. The 12-lead electrocardiogram (ECG) testing is commonly used at hospital for continuous heart rate monitoring. Although ECG has high accuracy and can provide detailed information about cardiac activity, the need of professional nursing personnel for the placement of electrodes makes it difficult to use out of hospitals. Besides, the wiring configuration

of the device obstructs patients' daily activities. And it takes time for the nursing personnel to sterilize the skin (sometimes shaving involved), attach electrodes and hook up the cables.

Respiratory efforts create deformation of the chest wall. As the volume of the thoracic cavity increases and decreases due to inhalation and exhalation, rib cage expansion and contraction will create a displacement of the chest wall as well as variation in chest circumference. Respiratory activity related signal, such as respiratory waveform or respiratory rate, can be measured through either respiratory belt or inductive plethysmography attached around the chest. The elevating and descending pattern observed in the respiratory waveform is directly associated with lung ventilation, which is an indicator of respiratory physiology [2]. The rates can be stored and estimated over certain period of time, which can be used for diagnosis. However, it is not always the case when a chest belt could be used for respiratory effort monitoring. For example, it cannot be an ideal method for burnt injury patients. When it comes to everyday use, the discomfort or excessive pressure it may cause could interfere the integrity of the respiration pattern, yielding unreliable readings.

Consequently, a user-friendly and reliable device for heartbeat and respiration monitoring is of great potential in medical instrumentation innovation.

1.2 Contribution

This work presents a bio-impedance analysis (BIA) based heart rate sensing method, and a non-contact Wi-Fi band Doppler radar based method. The contact sensing methods with BIA only used 4 electrodes to measure heart rate from subject's wrist. The accuracy was evaluated and confirmed by comparing with the heartbeat signal concurrently measured from a commercial finger pulse transducer, which validates the feasibility of the proposed BIA system. The author also explored the feasibility of multiple other biosensors, based on various kinds of measurement principle for heart rate sensing and respiratory rate monitoring. Each sensor was tested on more than one locations over the subject's body and repeated multiple times to validate the results. It was the first reported attempt to detect such vital signs from locations such as upper arm and wrist with non-conventional biosensors. A novel BIA-based board level sensing platform was also designed and fabricated. The first attempt in the heart rate sensing was successful. Future work on the sensing board involves further debugging, circuitry optimization and miniaturization.

Doppler radar based non-contact sensing was another area that this thesis focuses. It was intended to discern small displacements of a periodically moving target, which potentially could be used on measuring body surface movements to extract physiological parameters associated with cardiac activities. For example, the time dependent variations of chest wall indicate the impact of the heartbeat motion over diastolic and systolic cycles, thus applicable for heart rate extraction and related health issue prognosis. The lead free configuration eliminates the wiring issue commonly suffered with ECG system, yet provides a reliable reading on heart rate measurement to gold standard. It is proven to be a good candidate for non-contact physiological monitoring.

1.3 Thesis organization

Chapter 1 has presented an overview of the importance of physiological monitoring system for vital sign measurement and focused on heart rate and respiration monitoring. Discussions on conventional instrumentation for these two types of vital sign monitoring and their issues were presented. User-friendly, novel contact and non-contact methods in detecting weak physiological parameters were proposed, and a summary on the contributions of the thesis was addressed.

Chapter 2 discusses conventional contact and radar-based non-contact sensing methods used for physiological parameters monitoring. The measurement principle, common configurations, commercially available products and a list of recent work were demonstrated and compared.

Chapter 3 demonstrates the fundamentals on bio-impedance analysis, the principle of heartbeat sensing it based on, and proposed system. Institution Review Board (IRB) approved human testing data were collected, and compared with reference for accuracy evaluation. It was the first reported BIA heartbeat monitoring system in the wristband configuration.

Chapter 4 covers an extensive investigation on conventional biosensor detecting heart rate and respiratory rate over non-conventional locations on human body. An introduction of the sensors involved and their common settings were given, followed by an overview of interested testing locations. The measurement results in spatial and spectrum domain demonstrate the performance of vital sign detection, which are summarized at the end of the chapter.

Chapter 5 demonstrates first micrometer resolution Wi-Fi band Doppler radar for sub-millimeter physiological displacement measurement. It is intended for estimating small displacements on the body surface resulting from cardiac activity. A mechanical mover was used

as target, and programmed to conduct sinusoidal motions to simulate pulse motions. Measured displacements were compared with a reference system, which indicates a superior performance in accuracy for having absolute errors less than 10μm, and relative errors below 4%.

Chapter 6 summarizes the main contributions of the thesis and matches with the conclusions. A list of topics of future work as expansions of some of the preliminary studies is provided.

Chapter 2. Literature Review

2.1. Contact sensing

The Electrocardiography (ECG) is a diagnostic process commonly performed in hospital to assess electrical activity of heart over a period of time using electrodes placed on the skin. A standardized 12-lead ECG system contains ten electrodes, among which four are placed on limbs and six are placed on the chest wall (Figure 2.1). These electrodes are able to provide electrical views of heart from 12 different angles. By interpreting the recorded tracing, a large amount of information about the structure and electrical function of heart can be obtained. For monitoring heart rate, it is obvious that 12-lead ECG is too abundant. In this case, the ECG measurement system can be simplified to 3 leads.

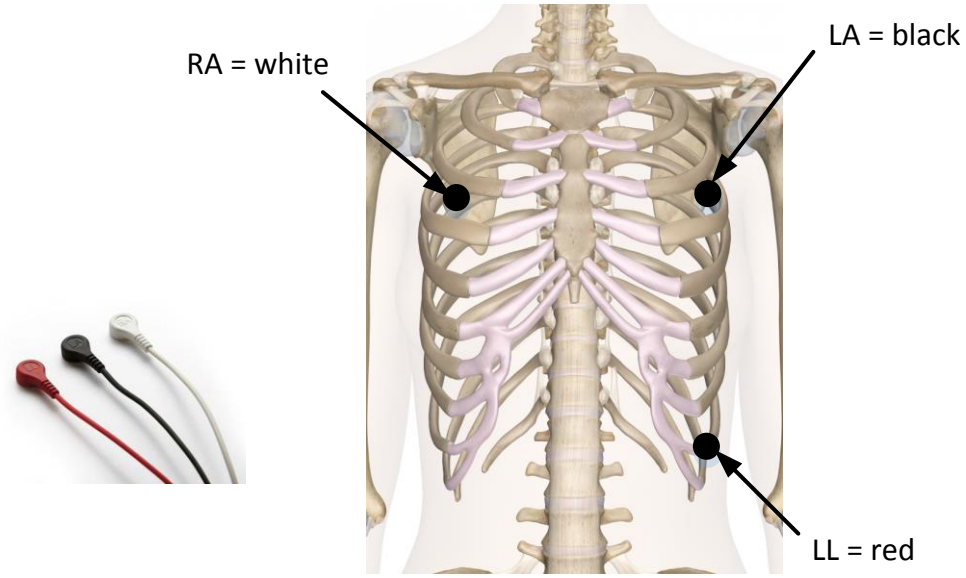

Figure 2.1 3-lead ECG configuration

Piezoelectric-based sensors have been studied by many researchers. This kind of sensor produces a voltage when subjected to a physical stress or strain (Figure 2.2(a)). Piezoelectric-based sensors can be fabricated with kinds of materials, such as crystals and certain ceramics, for different applications. Due to the property of the accumulation of electrical charge in response to deformation, some researchers applied piezoelectric sensors to harvest the energy from human body [3]-[5]. Also the property of high sensitivity to strain makes piezoelectric sensors popular in physiological monitoring [6]. In [7], a piezoelectric sensor embedded wearable system in the form of necklace was proposed to detect skin motion in the lower trachea during ingestion. The piezoelectric sensor was also used to acquire arterial pulse signal from radial artery on wrist [7] and neck [8]. In [9], a piezoelectric sensor was put under the mattress to monitor vital signs (both respiration and heart rate) continuously. Figure 2.2(b) gives some samples of piezoelectric pieces.

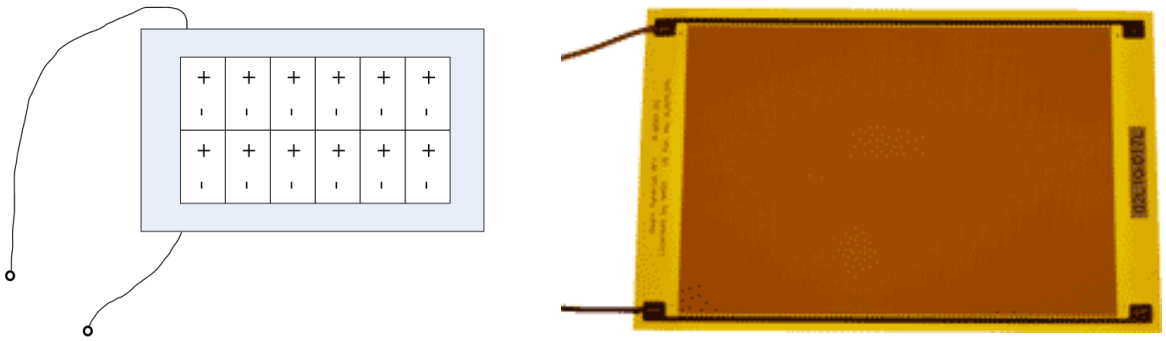

(a) (b)

Figure 2.2 (a) A demonstration of sensor with piezoelectric effect. (b) Samples of piezoelectric pieces

Another increasingly popular way for vital signs measurement is known as photoplethysmography (PPG), especially in the form of wearable devices. The PPG technique recognizes the pulse wave by illuminating a light-emitting diode (LED) light on the skin and then measuring either the reflected or transmitted light intensity by a photodetector (PD). The two types of PD placement – transmissive and reflective - are shown in Figure 2.3. The changes in light intensity are corresponded with small variations of the blood volume and provide the information

on heart rate. Based on optical characteristics of lights and absorption level of biological tissues, infrared (IR) or near-infrared light and green light are commonly used in PPG sensors. IR or near-IR light is suitable for measuring deep-tissue blood flow with transmissive mode. Green light is better for the measurement of superficial blood flow in skin with reflective mode [10]. Several consumer devices available on the market to monitor heart rate are based on green-light PPG, such as Apple Watch, MIO Alpha, Fitbit Wristband, etc.

(a) Transmissive way of PD placement (b) Reflective way of PD placement

Figure 2.3 Transmissive and reflective ways

Although several green-light-based PPG heart rate monitoring devices have already been available commercially now, research on optimizing PPG measurement is still popular and necessary. Extensive studies have been conducted for PPG sensors measurements on different sites, including index finger [11], wrist [12]-[14], brachia [15][16], ear [17][18], neck [19], forehead [20]. Besides, motion artifacts caused by random body movement mainly consist of low-frequency components, which might overlap with pulse signal and interfere heart rate measurement result. Therefore, an effective signal processing algorithm for motion artifacts reduction is necessary. One of widely used techniques for removing motion artifacts is adaptive filtering which needs a suitable reference signal. Signal decomposition is shown recently to be a powerful approach to remove motion artifacts. Recently, the widely used techniques for removing motion artifacts include independent component analysis (ICA) [21], adaptive filter [22][23], signal decomposition [24][25], etc.

Bio-impedance analysis (BIA) is also a potential contact sensor worth being studied due to its noninvasive feature, low cost, and portability. Many researchers have conducted studies on bio-

impedance analysis and applied it in a wide range of areas, such as physiological variables monitoring (e.g. heart rate [26] and respiratory rate), tissue state assessment [27], detection of ischemia [28] or cancer cells [29], etc. In cardiovascular studies, bio-impedance measurements enable the acquisition of information on stroke volume [30]. [31] employed BIA to measure the pulse wave velocity (PWV) from the radial artery in the wrist to the middle finger. In [32], researchers combined BIA, ECG and continuous wave (CW) radar together to measure pulse transit time (PTT) at the central arteries for estimating cuffless blood pressure. In [33] and [34], heart rate was detected from bio-impedance variation on feet by standing on a bathroom weighing scale intended for body composition measurement. These systems were easy to use but its configuration limited the possibility of continuous heart rate monitoring. [35] measured heart rate on the wrist based on bio-impedance analysis with electrodes placed along the artery.

2.2. Radar-based non-contact sensing

2.2.1. Non-contact physiological sensing

Radar based physiological monitoring has been demonstrated in many studies for the feasibility of vital sign detection and physiological monitoring. Its wireless sensing capability eliminates electrodes attachment and offers comparable readings on a number of physiological parameters. Researchers have proved the feasibility of measuring respiration rate and heart rate via various types of radar, such as continuous-wave (CW) [36][37][38], frequency-modulated CW (FMCW) [39][40], pulse [41][42] radars. Tidal volume change was found to be linearly correlated to chest wall displacement, which was detectable by CW Doppler radar under DC coupled mode [43][44]. From reconstructed respiratory signal, Doppler radar was able to extract indices of heart rate variability (HRV) and respiratory sinus arrhythmia (RSA) [45]. Palpable physiological movements over the skin surface or even beneath can also be detected with Doppler radar. Non-invasive arterial pulse wave measurement was first reported in [46] by sensing arterial wall movement from three different sites. A non-contact PWV sensor was developed by simultaneously measuring pulse-related displacement over breath-holding chest wall and lower limb under calf pressure [47]. Similar principle was applied by using an ultra-wide band (UWB) radar sensor to measure PWV between brachial artery and foot [48].

The feasibilities of cardiopulmonary, arterial, and mechanical activity detection using microwave Doppler radar enable tracks of various practical applications, such as fall detection

[49], respiratory pattern analysis [50], sleep study [51], occupancy sensing [52][53], in vivo tumor targeting and speech monitoring [54]. Due to its penetration ability, Doppler radar signal not only can go through clothing or skin surface for physiological parameter detection, it is also able to penetrate concrete walls or obstacles for through-wall sensing and rescue operations [55][56][57]. Tissue sensing of the medical radar system utilize the penetration feature and enables 2D imaging of the area of interest [58]. Some of the pioneer work have presented achievements in breast imaging [59], breast cancer detection [60].

2.2.2. Physiological parameter extraction

In general, cardiopulmonary activities create periodic deformation on chest wall, the time varying displacement of which in superior-posterior direction ranges from 4mm to 12mm for respiration [61], and 0.035mm to 1mm for heartbeat [2]. The extraction of displacement information holds the key to vital sign signal reconstruction, which depends on full phase recovery. If physiological rate information is desired, single channel radar receiver is sufficient because phase changes are proportional to amplitude variation of the reflected signal [62][63]. From the temporal characteristics of baseband signals, the rate of respiration or heartbeat is accessible by counting total peaks in the waveform in given time. Spectral analysis is another option by performing Fourier Transform and converting the signals to frequency domain, where the most significant peak's frequency indicates the rate.

If accurate displacement over time is to be assessed, arctangent demodulation (AD) reported in [64][65][66], as well as complex signal demodulation (CSD) introduced in [67] can be used. The CSD method has the advantages of simple radar architecture, calibration-free and self-verification. It employs single-channel homodyne receiver and resolves displacement in frequency domain. The difficulty lies in its rigorous mathematical analysis, yet the minimum displacement detectable is limited to one third of the carrier wavelength for fixed frequency radar. Reported measurement resolution is around 50μm for 2mm sinusoidal movement. When the AD method is applied, quadrature receiver is needed. Its in-phase/quadrature-phase (I/Q) outputs are processed concurrently to demodulate phase information, which can be used to recover displacement in time domain. The challenge associated with AD method is the necessity of center estimation, dc-offset removal and data calibration. A heuristic estimator based center estimation method [68][69], a Levenberg–Marquardt method based circle fitting approach [70], and a dispersion minimization

method [65] are the most prominent methods for quadrature Doppler radar related center estimation. Though [70] and [65] outperforms [68][69] in accuracy of finding arc center while spanning a wide phase rotation angle according to [71], limited angle still poses a challenge to all three methods. This is especially crucial for 2.4GHz radar system measuring weak physiological displacements. In [72], radius correction method was introduced for calibrating I/Q transcribed arc in cases when detected target displacement is relatively small. In [65] and [70], hardware calibration method was discussed that involves I/Q imbalance error estimation and compensation. The only published chest displacement from heartbeat was found in [66], which enabled the detection of sub-millimeter scale results using a network analyzer at three transmitting frequencies. However, the measurements were conducted without a reference to compare its accuracy with.

2.3. Summary

This chapter summarized some of the contact sensing principle and instrumentations, including ECG, plethysmography, PPG, piezoelectric-based sensor and BIA. Their performances in vital sign sensing were analyzed and compared. Some of the recent advances in using these sensors for physiological sensing and wearable applications were presented. Radar based physiological monitoring was also demonstrated in many state-of-the-art works for the feasibility of vital sign detection and physiological monitoring. Detailed information on displacement extraction, the approaches and their performances were briefly overviewed.

Chapter 3. Bio-impedance Based Physiological Monitoring

3.1. Introduction to Bio-impedance Analysis

Bio-impedance refers to the electrical properties of biological tissues, which are primarily composed of cells and fluids. A cell is formed by a membrane enclosing cytoplasm inside. The cell membrane isolates the Intracellular (IC) medium from the Extracellular (EC) medium. The equivalent electrical impedance model of blood cells is illustrated in Figure 3.1. The resistance of the inner part of the blood cell is denoted in R_i, while R_e represents the resistance of the extracellular medium. The cell membrane behaves as a capacitor, which is represented in C_m. Due to the resistive and reactive behavior of each component, electrical current that passes through blood cells behaves differently according to frequencies. The current at low frequencies will flow mainly through the extracellular medium. At higher frequencies, the modeled cell membrane capacitor will act as shunt that allows current flow through intracellular medium of blood cells.

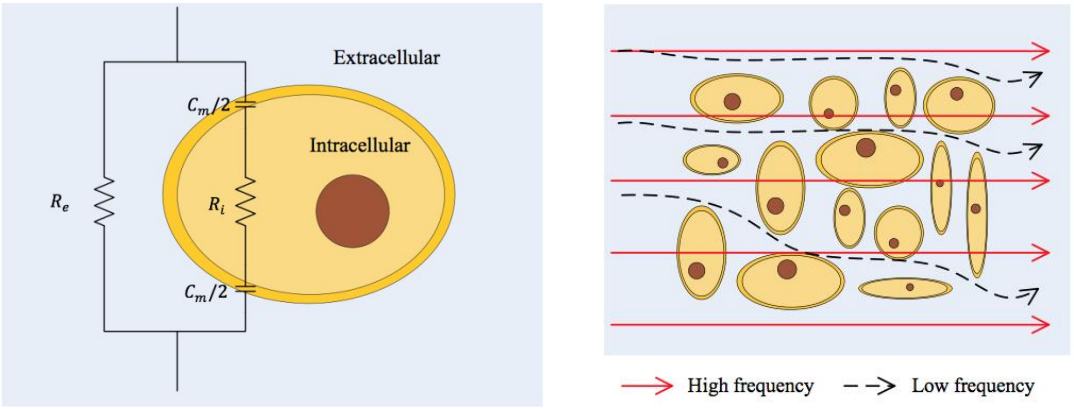

(a) (b)

Figure 3.1 (a) Electrical model of blood cells. (b) Flow paths of alternative current with different frequencies.

Bio-impedance analysis (BIA) is a widely used method for body composition measurement, i.e. estimating fat, muscle, bone and fluid levels in the human body. By injecting a small constant alternating current into human body, the voltage across designated locations is measured. And the impedance is obtained by applying Ohm's Law. The chosen excitation current should ensure users' safety and the effectiveness of measurement.

Four-electrode (tetrapolar) configuration is commonly used in bio-impedance measurement, where two electrodes known as driving electrodes are used for sending current into human body, and the others are called sensing electrodes for obtaining voltage across designated locations. Figure 3.2 shows the 4-electrode configuration of body composition measurement using bio-impedance analysis.

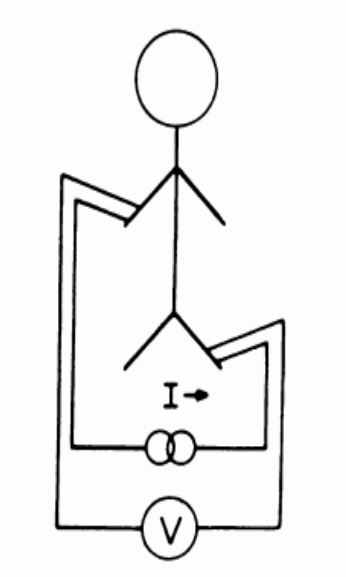

Figure 3.2 4-elecrode configuration.

3.2. Heartbeat measurement principle based on BIA

When heart pumps blood from chamber, there is a pulse wave flowing throughout the whole body via the circulatory system. This propagation of blood flow causes a small variation of bio-impedance change on a localized area of human body. It has been reported that low-level heart

beat associated impedance variations can be measured in limbs [73]. Heart rate thus can readily be detected from wrist by measuring such impedance variations. As shown in Figure 3.3, Z_0 indicates the constant impedance of wrist tissues, and ΔZ(t) represents the impedance variations directly related to heartbeat.

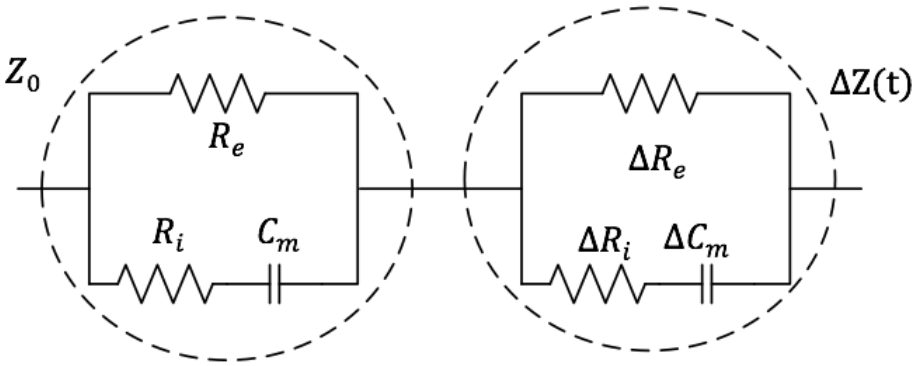

Figure 3.3 Electrical impedance model for blood including impedance variation related to heartbeat [73].

To measure impedance of a small area on wrist, 4-electrode configuration will be used, as shown in Figure 3.4. When a small constant alternating current is sent through two driving electrodes (represented as red dots), the resulting voltage signal across the sensing electrodes (represented as black dots) is expressed as

$$V(t)=(Z_0+\Delta Z(t))I_0\cos(w_0t) \tag{3.1}$$

where $I_0cos(w_0t)$ is a small AC current with constant amplitude injected into the wrist. From (3.1) it can be seen that measured voltage $V(t)$ is a sinusoidal signal whose amplitude is modulated by the impedance variation resulted from heartbeat pulses. With appropriated signal processing method, the small variation of impedance ΔZ(t) can be extracted.

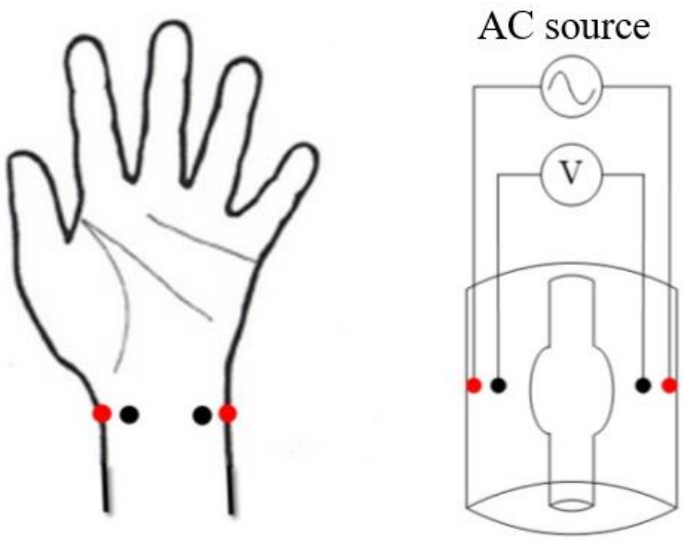

Figure 3.4 Wrist model and tetra-polar configuration for bio-impedance sensing, where red dots represent driving electrodes and black ones represent sensing electrodes [74].

3.3. Measurement system design

The proposed architecture of bio-impedance measurement system is shown in Figure 3.5. Instead of directly demodulating the output signal for $\Delta Z(t)$, a down-converting structure with a mixer is used, which is similar to the direct conversion in the radar receiver. A constant alternating current with an amplitude of 425μA and a frequency of 50kHz is injected through driving electrodes. The amplitude and frequency of the applying current is generated by a standard bio-impedance analyzer so that the system is able to detect low-level impedance variations without harming human subject [75].

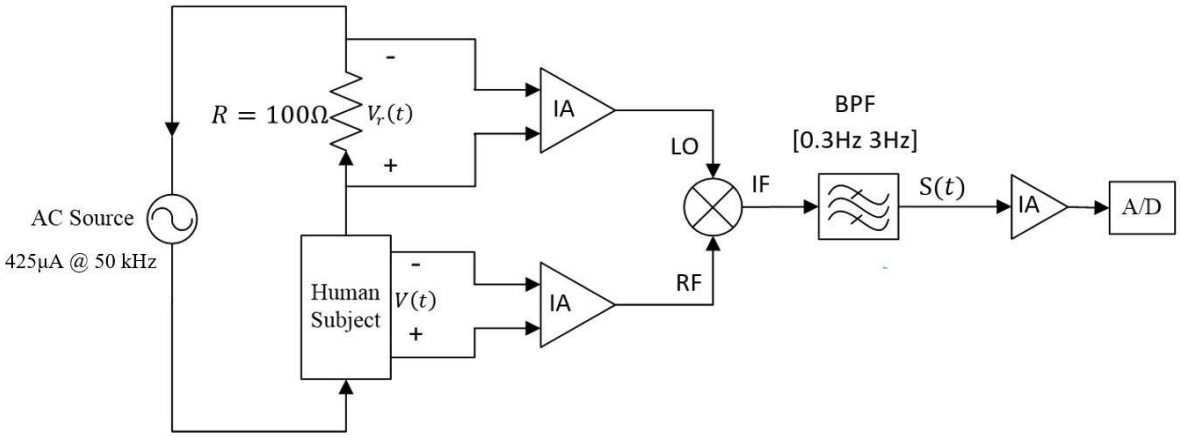

Figure 3.5 Block diagram of heart-related impedance variation measurement.

The resistor R in series with the human body is to obtain the local oscillator (LO) signal. The reason of using the resistor of 100Ω is that the parallel connection between R and the input impedance of instrumentation amplifier (IA) has minimal affection on the actual voltage across the resistor R. Thus, the voltage across it can be represented as

$$V_r(t) = RI_0 \cos(\omega_0 t) \tag{3.2}$$

High-gain amplification is desired for both voltage signals because the impedance variation is on the order of mΩ and the corresponding voltages change is on the order of μV when a 425μA of AC current is applied. Sufficient amplification of these two voltage signals not only can increase the accuracy of the measurement, but also can effectively reduce the conversion loss of the mixer. The amplified Vr(t) and V(t) are sent to LO port and radio-frequency (RF) port of a mixer, respectively. After mixing them, the intermediate frequency (IF) signal is obtained at IF port, which is

$$\begin{aligned} IF &= G_1 RI_0 \cos(w_0 t) \times G_2 (Z_0 + \Delta Z(t)) I_0 \cos(w_0 t) \\ &= GR(Z_0 + \Delta Z(t)) I_0^2 \cos^2(w_0 t) \\ &= \frac{G}{2} I_0^2 Z_0 R + \frac{G}{2} I_0^2 \Delta Z(t) R + \frac{G}{2} I_0^2 R(Z_0 + \Delta Z(t)) \cos(2w_0 t) \end{aligned} \tag{3.3}$$

where G_1 and G_2 are the gains of the IA following the resistor R and the human body respectively, and $G = G_1 G_2$.

The bandpass filter is used to remove the DC offset related to basal impedance Z_0 and the double-frequency component in the mixer output. By sending the IF signal into the bandpass filter with the corner frequency of 0.3Hz and 3Hz, the heart-related signal S(t) can be obtained, which is

$$\begin{aligned} S(t) &= \cancel{\frac{G}{2} I_0^2 Z_0 R} + \frac{G}{2} I_0^2 \Delta Z(t) R + \cancel{\frac{G}{2} I_0^2 R(Z_0 + \Delta Z(t)) \cos(2\omega_0 t)} \\ &= \frac{G}{2} I_0^2 \Delta Z(t) R \end{aligned} \tag{3.4}$$

Since the impedance change related to heart pulse wave is very small, a high gain amplifier is necessary before S(t) is sent to analog-to-digital converter (A/D).

3.4. Experiment set-up

Before turning the proposed bio-impedance measurement system into a full printed circuit board (PCB) circuit, an initial experiment was conducted to validate the feasibility and accuracy of this architecture for extracting heartbeat signal. The RJL Quantum II Bio-impedance Analyzer was used as the AC source for desired constant alternating current. Covidien CA-610 electrodes were placed on the wrist for current driving and voltage detection. The electrodes were attached to the same side of the wrist, which were perpendicular to the artery like a wristband. Both upper and lower wrists were tested for validation. Figure 3.6 shows the settings of electrodes. The pair at the two ends induced AC current through the wrist, while the pair in the middle with 3.7cm separation from their centers were used to sense voltage across their locations. A Model 1010 piezoelectric finger pulse transducer was attached on the index finger of the subject to obtain a reference pulse signal synchronously. To build the direct conversion architecture, a 100Ω resistor was connected in series with the subject that served as the local oscillator (LO) source. When running the same current through the subject and the resistor, voltage signals sensed across them will have the same frequency and phase, which were fed to mixer input ports after proper conditioning.

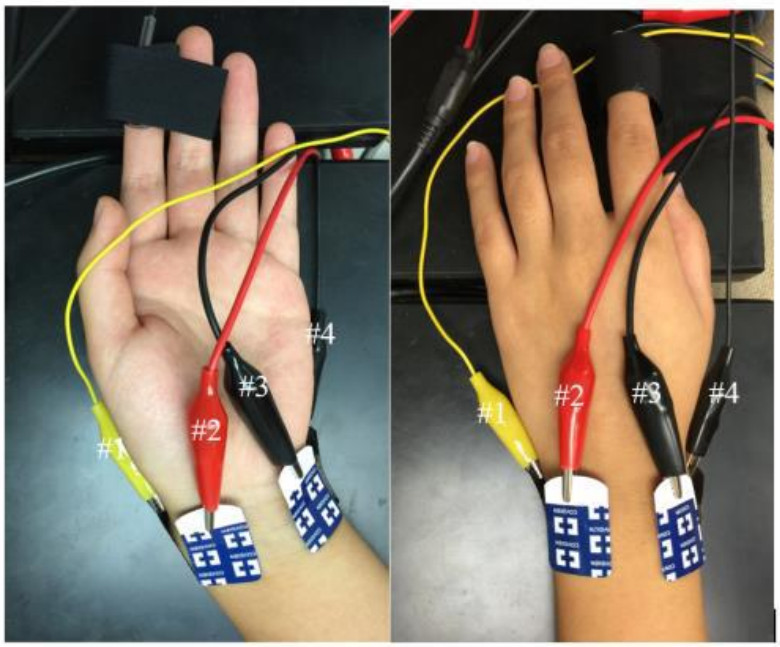

Figure 3.6 Settings of electrodes

The amplification of the voltage signals were achieved by Stanford SR-560 low-noise amplifiers (LNA). They also performed filtering function in order to rule out noises in these two channels. For human subject induced voltage signal (RF), it was amplified by 50 times after a band-pass filter with cutoff frequencies at 10kHz and 100kHz. As for the resistor voltage (LO), it was amplified by 200 times, and band-pass filtered at same cutoff frequencies. Both of the signals were AC coupled in SR-560 to remove DC. After the low-noise amplifier (LNA), human subject's AC voltage was fed to radio frequency (RF) port of a mixer (Mini-Circuits ZLW-6+), while the resistor's AC voltage was fed to the LO port for mixing. The intermediate frequency (IF) port output the mixed components to a band-pass filter. The function of the BPF was to remove double frequency components in the mixer products, leaving only the baseband signal that contained heartbeat related signal. The BPF's cutoff frequencies were selected to be 0.3Hz-3Hz, which was realized by another SR-560 LNA. The filtered signal was AC coupled as well, and amplified by 50 times to increase its resolution. The final heart beat related signal demodulated from mixer and the finger pulse signal were sent to NI USB-6218 for analog-to-digital conversion, and further processing was performed in MATLAB.

3.5. Human testing results and discussions

The experiments were conducted according to the Committee on Human Studies (CHS) under protocol number 19176 and HRPO A-18177. In the conduct of research where humans are the subjects, investigators adhered to the policies regarding the protection of human subjects as prescribed by Code of Federal Regulations (CFR) Title 45, Volume 1, Part 46; Title 32, Chapter 1, Part 219; and Title 21, Chapter 1, Part 50 (Protection of Human Subjects).

Two subjects were recruited in this study. Experiment results of subject #1 from lower wrist are presented in Figure 3.7. It can be seen from Figure 3.7(a) that there is power line noise in the raw bio-impedance signal. But it is evident that the envelope of the bio-impedance signal is in good agreement with the finger pulse signal. After filtering and peak detection of bio-impedance signal in MATLAB, there are 35 peaks detected in both finger pulse and bio-impedance signals during the 30-second duration. Thus, the heart rate acquired from BIA system is 70BPM (beats per minute), which matches its reference.

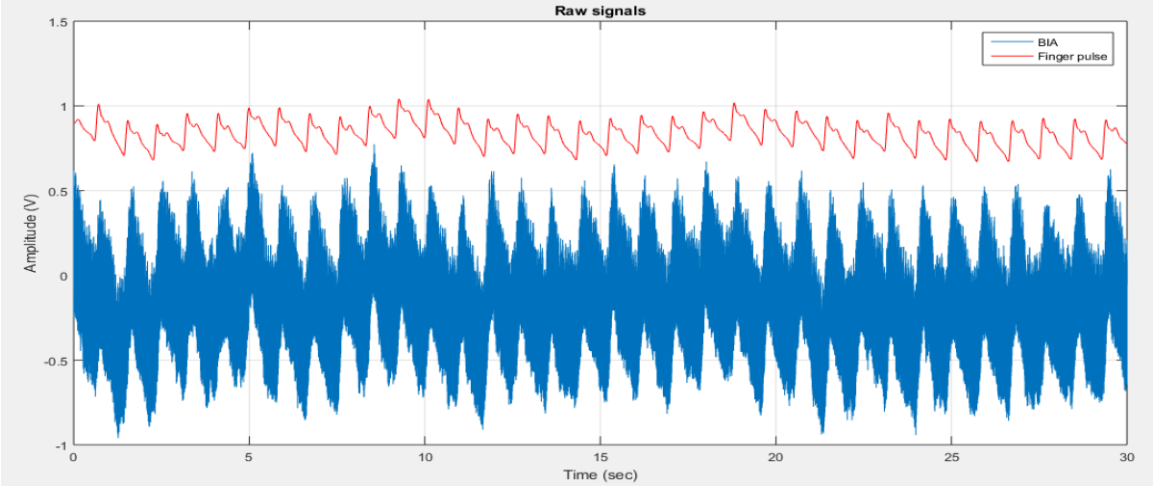

(a)

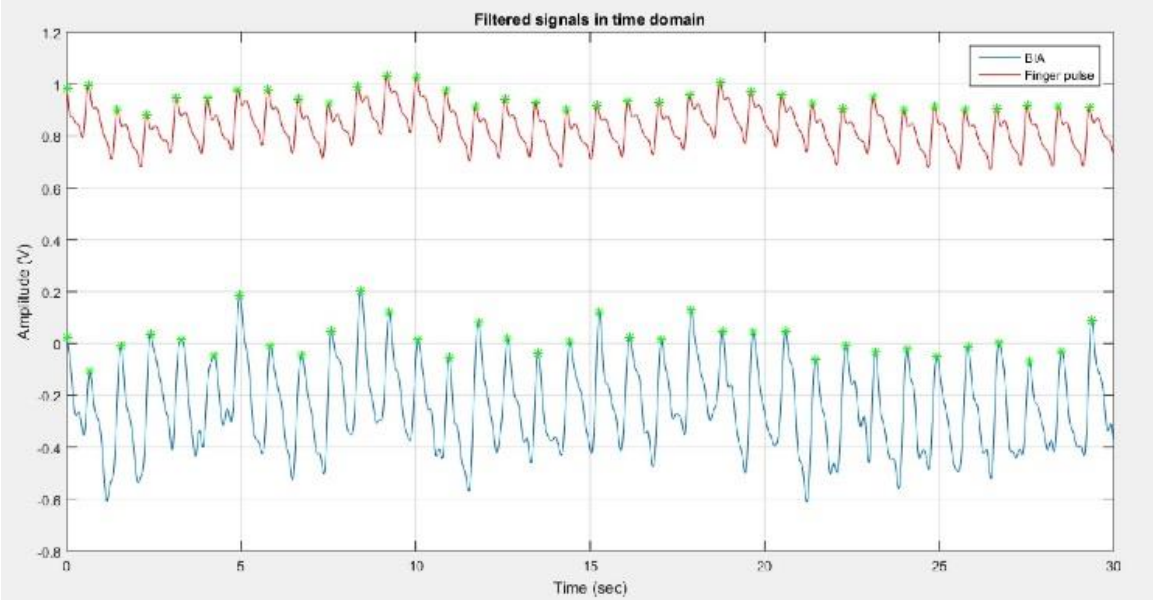

(b)

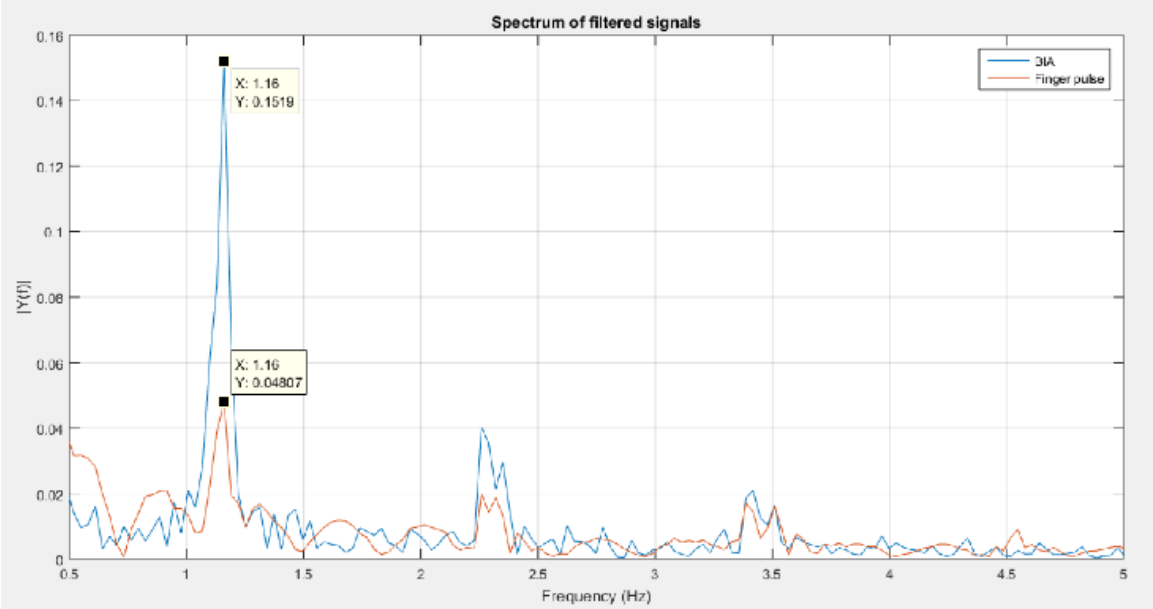

(c)

Figure 3.7 Experiment results of subject #1 from lower wrist (a) (b) (c)

From the spectrum plots of the two signals shown in Figure 3.7(c), it can be seen that accurate heart rate can also be obtained, which is $1.16 * 60 = 70$BPM. The consistency of results obtained from both time and frequency domains indicates that (1) heart rate can be monitored from the lower side of wrist by measuring the heart-related impedance variation in a wristband

configuration; (2) direct down-conversion structure of bio-impedance measurement system is feasible.

The same experiment procedure was repeated on the upper side of wrist for the two subjects, which conforms with the same configuration as the lower wrist experiment. A summary of experiment results of subject #1 and #2 from both lower and upper wrist is listed in Table 3.1, where heart rates detected from the proposed monitoring system are obtained and compared with finger pulse transducer results. It can be seen that the bio-impedance measurement system yields reliable results that agree with the reference.

Table 3.1 Heart Rate Experiment Results

Configuration	**Subject**	**Heart Rate Measured**	
		Bio-impedance Measurement System	**Finger Pulse Transducer**
Lower Wrist	#1	70BPM	70BPM
	#2	64BPM	64BPM
Upper Wrsit	#1	70BPM	70BPM
	#2	64BPM	66BPM

3.6. Summary

In this chapter, a bio-impedance analysis based heart rate monitoring system was presented. The design used only four electrodes to sense heartbeat related signal on wrist where wristband is normally placed. Measurements were taken with the proposed setting and analyzed in time domain as well as on frequency spectrum. The measured results showed that impedance variation at wrist closely matched with the heartbeat signal acquired from a standard finger pulse transducer, which proved the feasibility of heart rate sensing by the system.

Chapter 4. Comparison of Contact Sensors

The location of sensor attachment is an important design issue that affects the signal quality and robustness against motion artifacts. Therefore, suitable attachment sites for different types of sensors must be located to optimize sensor performance. This chapter presents results of three sensors (ECG, PPG, and BIA) for measuring heart rate and respiratory rate on different body locations. Experimental data were analyzed in both time domain and frequency domain. A summary of the detection performance is consolidated at the end of the chapter.

4.1.Measurement overview

The bio-sensors tested, instrumentation and accessories involved are summarized in Table 4.1. Data acquisition system was also used to log measurement data for further processing.

Table 4.1 Summary on biosensors, instrumentations and accessories

Bio-sensor	Instruments	Accessory	Function	Test Sites
ECG	Biopac ECG100C	3M Resting ECG Electrodes	Electrical activity sensing	Front chest Side chest Back chest Upper arm
PPG	TI AFE4403 Watch EVM	N/A	Infrared sensing	Front chest Side chest Back chest Upper arm Upper wrist Lower wrist
BIA	RJL Quantum II Bio-impedance Analyzer, Amplifiers, Mini-Circuits Frequency Mixer	Kendall CA-610 Electrodes	Bio-impedance variation sensing	Front chest Side chest Back chest Upper arm Upper wrist Lower wrist

Reference measurements were conducted to verify the accuracy of each sensor. A Model 1010 piezoelectric pulse transducer was used to obtain heart rate reference signal at finger (Figure 4.1(b)). For that of the respiratory rate signal, an inductive plethysmography belt (Figure 4.1(a)) was used since the piezoelectric based chest belt (UFI Model 1132 Pneumotrace II, see Figure 4.1(c)) is unreliable in some cases due to firm contact requirement.

(a)

(b)

(c)

Figure 4.1 Reference sensors (a) Piezoelectric pulse transducer, (b) inductive plethysmography belt, (c) piezoelectric chest belt

4.2. Sensor measurement for heart rate and respiratory rate

4.2.1. Electrocardiogram (ECG)

3-lead ECG with Biopac ECG100C module was tested on four different sites: including three locations around the chest area (Figure 4.2(a)-(c)), and one location on the upper arm (Figure 4.2(d)). The illustrations in Figure 4.2 demonstrate locations where electrodes are placed. Since the ECG module requires three leads connection (+, -, and ground), the pad connected to ground lead is attached to the opposite side of the body for the first three sites at the same level, and the inner side of upper arm for the fourth site.

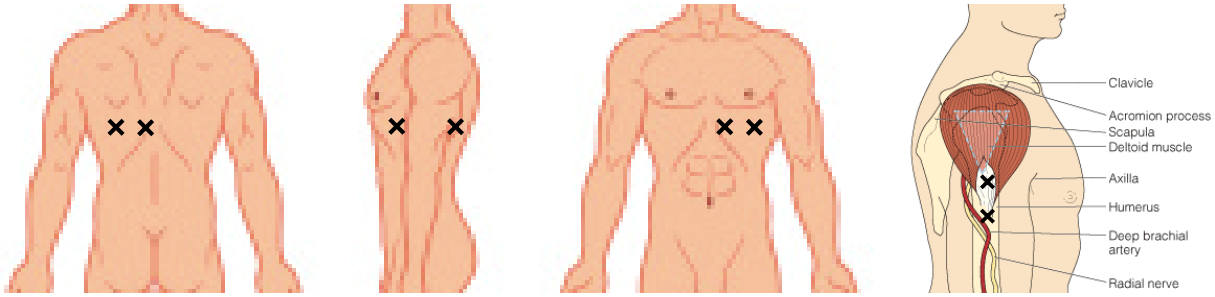

(a) (b) (c) (d)

Figure 4.2 Electrode positions of ECG testing. (a) chest front, (b) chest left side, (c) chest back, (d) upper arm

Biopac MP150WSW was used for data acquisition. The sampling rate was selected as 1kHz, with a gain of 5000. The piezoelectric pulse transducer was wrapped around subject's index finger to measure pulse concurrently as a reference. Measurement results are shown below.

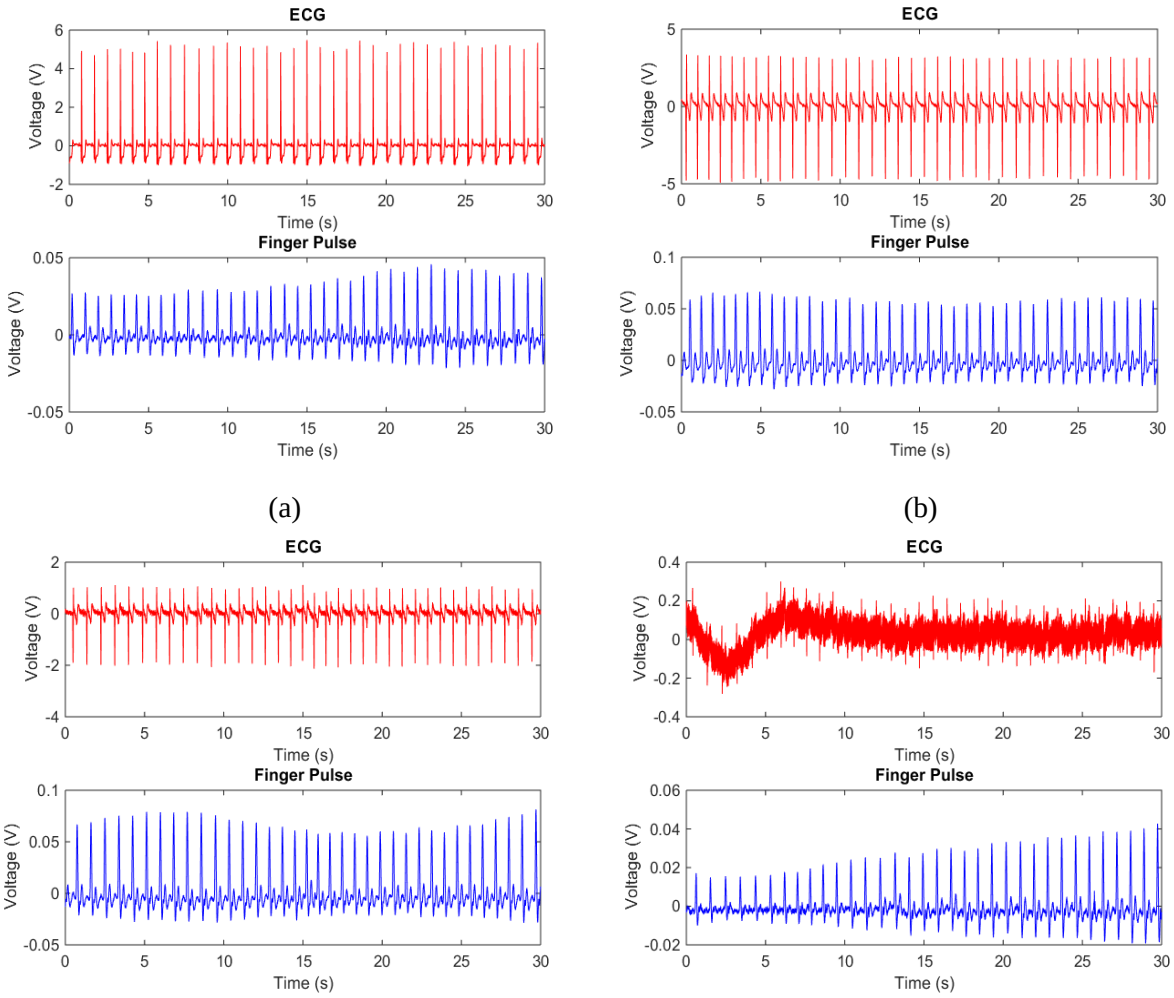

Figure 4.3 Time domain ECG measurement results in comparison with finger pulse sensor results. (a) chest front, (b) chest left side, (c) chest back, (d) upper arm.

Table 4.2 Heart rate measurement for ECG over chest and finger pulse transducer

ECG Electrode Location	ECG Heart Rate (beats in 30s)	Finger Pulse Heart Rate (beats in 30s)
Chest Front	35	36
Chest Left Side	37	37
Chest Back	36	36

Table 4.2 indicates a good agreement of ECG measurement to finger pulse reference. The slight time difference in each beat between measurement and reference is caused by geological difference.

ECG was measured from electrodes that are placed on the chest and upper arm, while finger pulse transducer measures the pulse at the tip of index finger. The pulse pressure wave takes time to propagate through a length of the arterial tree.

The time-domain performance of ECG on upper arm is inferior than the rest of the measurements, because it has a worse SNR and drifting. However, the Fast-Fourier transform (FFT) of ECG signal from upper arm and reference present a good agreement, shown in Figure 4.4. Both measurements obtain the same heart rate of 1.129Hz.

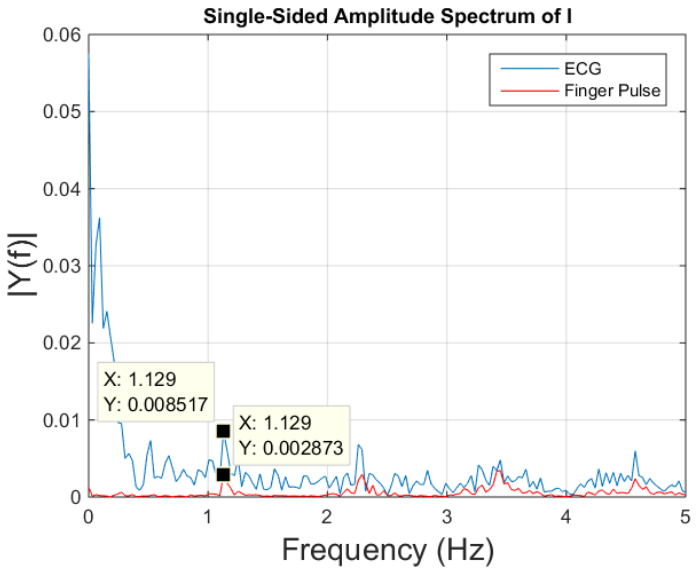

Figure 4.4 Frequency domain ECG measurement result of upper arm in comparison with finger pulse sensor.

4.2.2. Infrared wrist watch

TI AFE4403EVM watch works with AFE4403EVM GUI on PC to measure and record data. Figure 4.5 shows the photos of the watch, revealing its sensor location at the back and PC connector at side. Its inbuilt block diagram enables configuration of sample rates, sensing signal type, amplifier setting, and Infrared (IR) sensors selection. By adjusting these parameters, clear heart beat data can be obtained. AFE4403EVM GUI also allows us to export data into Excel files and further processing can be achieved in Matlab.

(a)

(b)

Figure 4.5 (a) Back view of the AFE4403 watch showing the infrared sensor. (b) Right-side view of the watch showing microUSB connector.

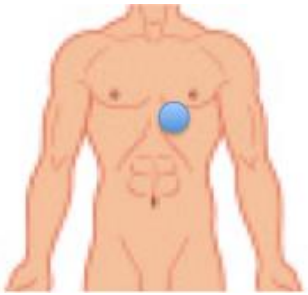

(a)

(b)

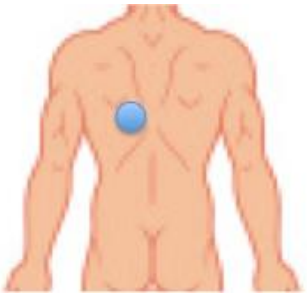

(c)

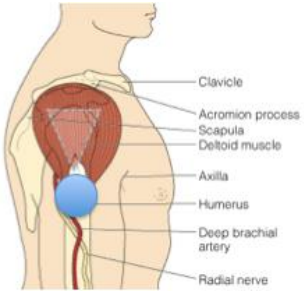

(d)

(e)

(f)

Figure 4.6 Testing locations for IR watch. (a) chest front, (b) chest left side, (c) chest back, (d) upper arm, (e) lower wrist, (f) upper wrist.

Six positions (front chest, side chest, back chest, upper arm, upper wrist, and lower wrist) were tested to measure heart rate and respiratory rate using infrared watch, shown in Figure 4.6.

The infrared watch was in tight contact with the skin and fixed with paper tape. Piezoelectric chest belt and finger pulse transducer were used to measure respiratory rate and heart rate concurrently as references. The infrared signal is sampled and recorded with AFE4403EVM GUI, whereas the reference signals are acquired with an NI USB-6218 data acquisition (DAQ) device. The NI DAQ was set with a delayed start time, which served as a time stamp to synchronize IR watch with references. However, it is possible that click on the start button of watch GUI for recording is not exactly on the same start time as the DAQ. Thus, there might be some slight time differences between infrared signals and reference signals. When doing the experiments, the subject put both hands on thighs while breathing normally in a relaxed state. Each measurement lasted 30 seconds.

Figure 4.7 – Figure 4.12 show the performance of infrared watch's heart rate measurement by comparing with reference in frequency domain, and its respiratory rate measurement in time domain.

From the spatial and spectrum representations, one can easily tell that heart rate can be measured from both sides of wrist, upper arm, and back chest. Whereas respiratory signal can be captured from all six locations, including the wrist locations, as validated by the bumps of IR signal in time domain corresponding well with those of the chest belt reference.

From an anatomical point of view, subject's chest expands during calm respiration and it will cause both shoulders move synchronously. When shoulders are lifted or relaxed, the arms and wrists will move in sync. Therefore, the respiratory rate can be measured from the upper arm and both sides of the wrist. Since such movement is relatively smaller than large body motion, pulse pressure wave that travels along the artery during each heart beat can be detected by the IR sensor, yielding accurate heart rate.

However, as for the measurements on front chest and side chest, heartbeat signal could be buried under the respiratory signal due to the large expansion on the chest. Therefore, it is difficult to extract heart rate from these two locations. When it comes to the back chest, since the expansion of back chest is relatively smaller than that of front and side chest, both rates can be measured at the same time.

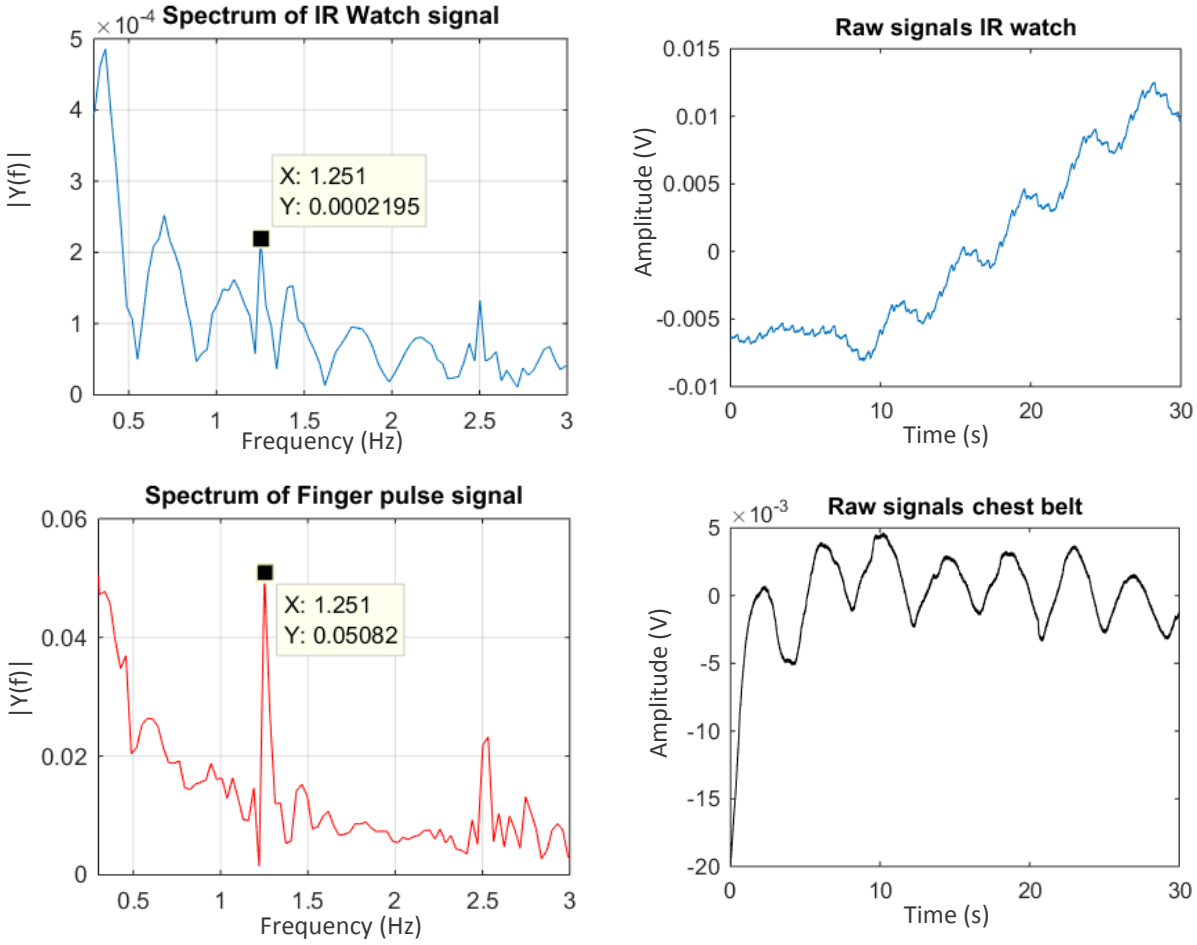

(a) (b)

Figure 4.7 Upper wrist measurement results with IR watch. (a) heart rate in frequency domain (b) respiratory rate in time domain.

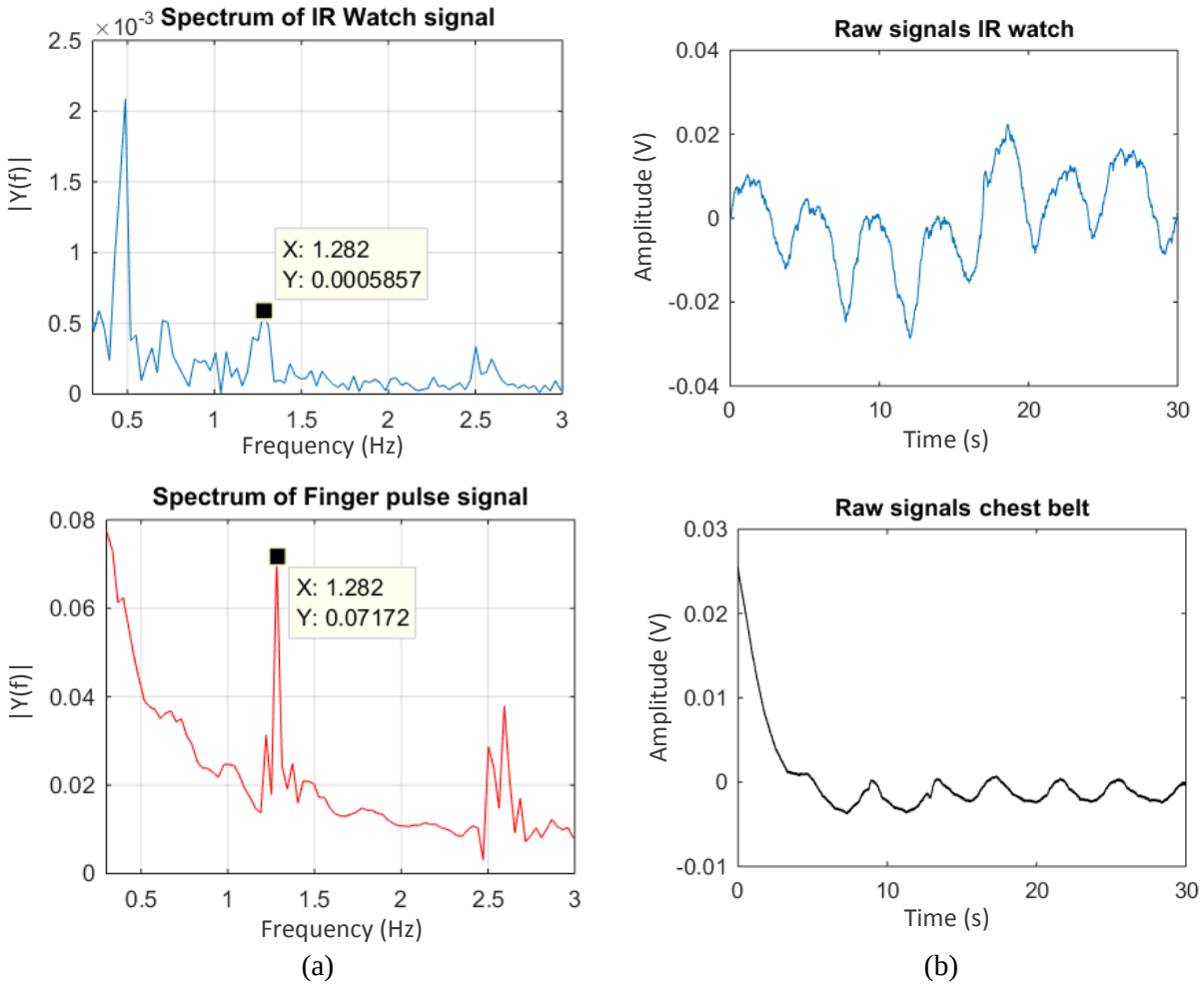

(a) (b)

Figure 4.8 Lower wrist measurement results with IR watch. (a) heart rate in frequency domain (b) respiratory rate in time domain.

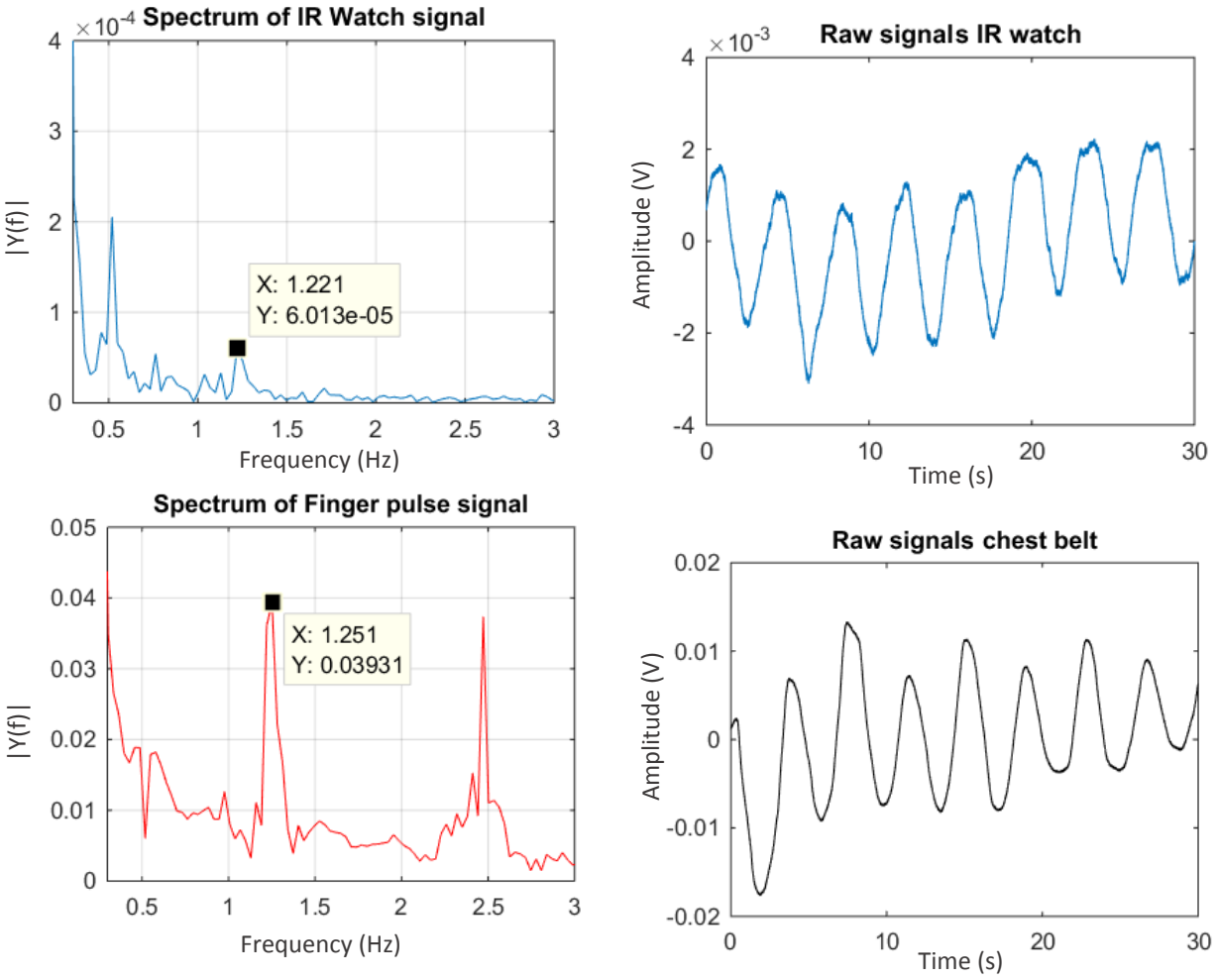

(a) (b)

Figure 4.9 Upper arm measurement results with IR watch. (a) heart rate in frequency domain (b) respiratory rate in time domain

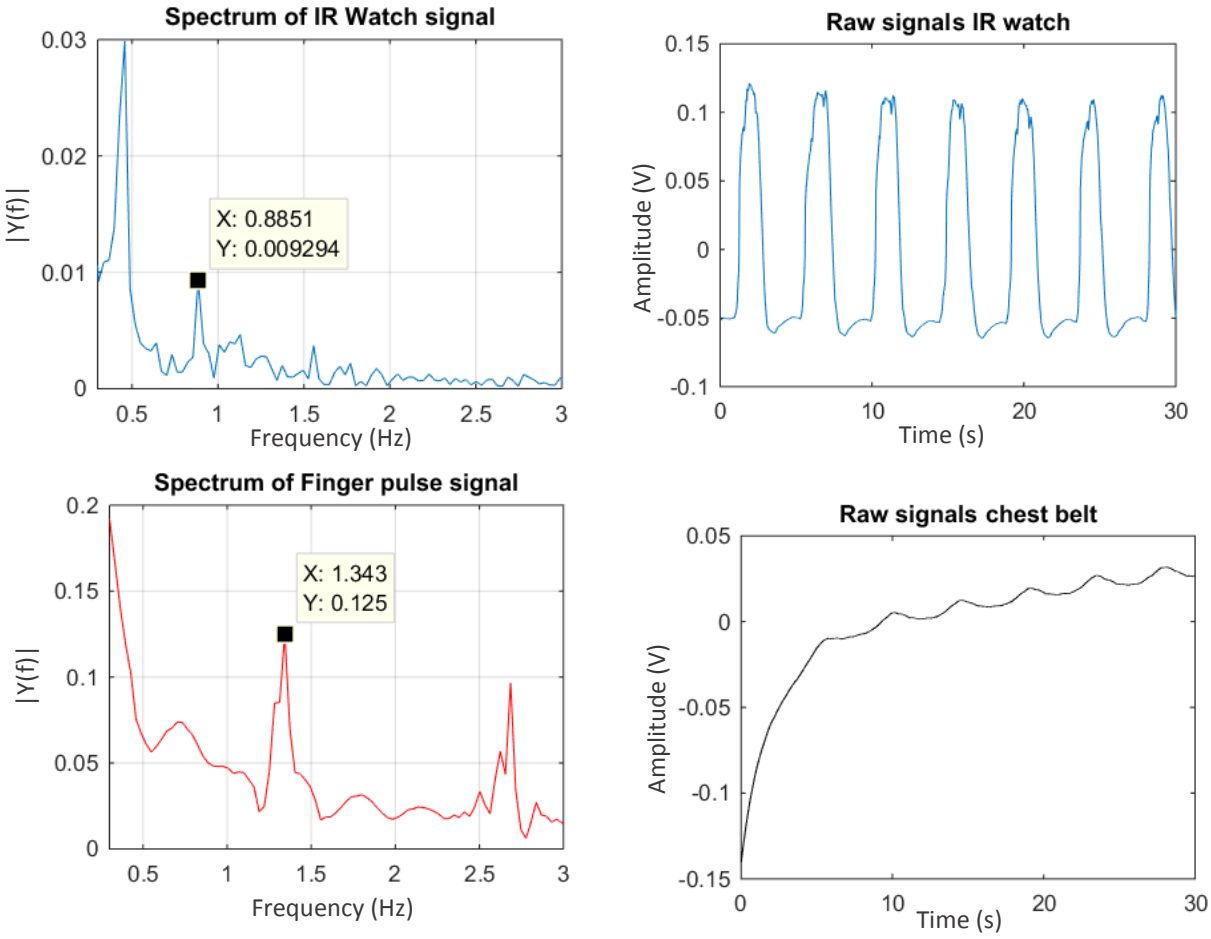

(a) (b)

Figure 4.10 Front chest measurement results with IR watch. (a) heart rate in frequency domain (b) respiratory rate in time domain.

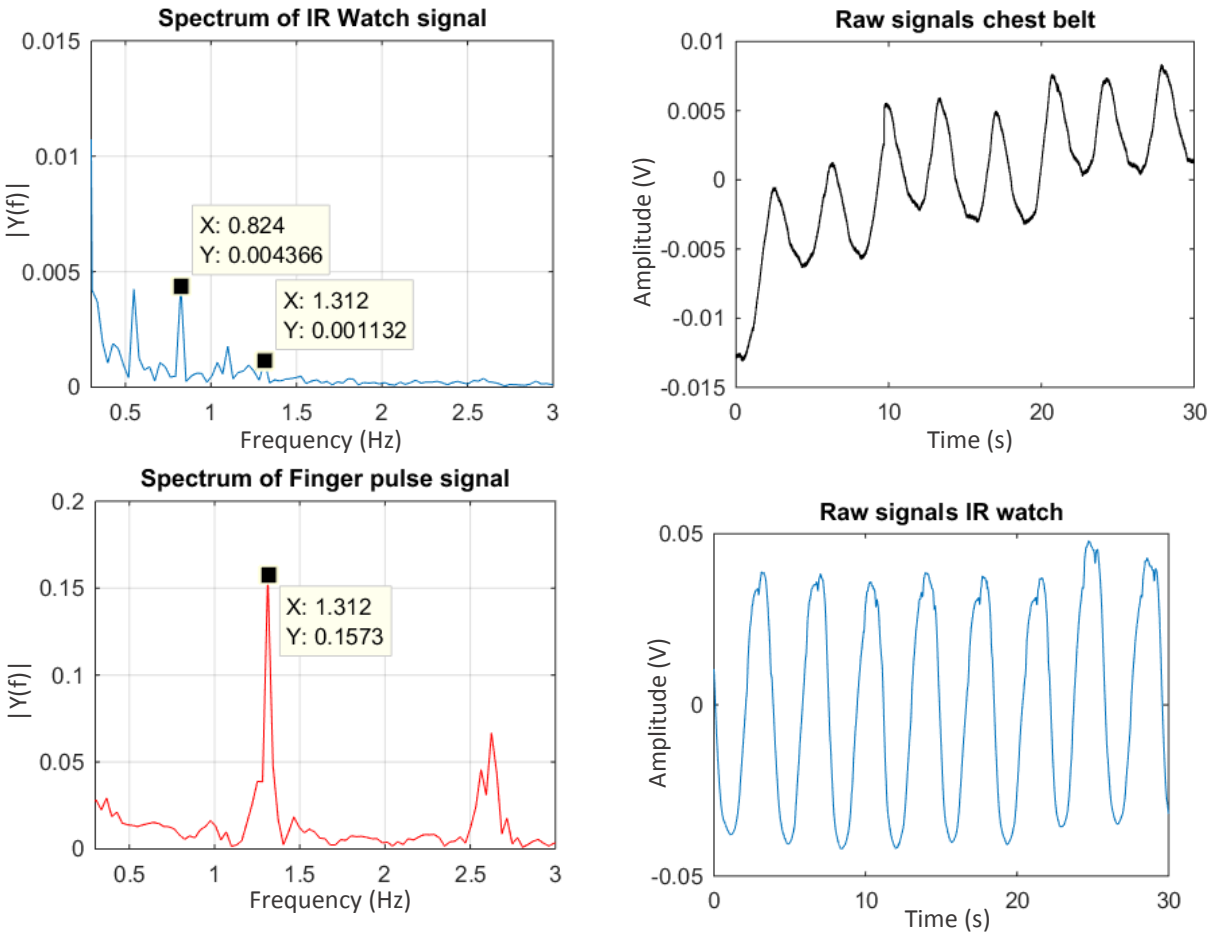

(a) (b)

Figure 4.11 Side chest measurement results with IR watch. (a) heart rate in frequency domain (b) respiratory rate in time domain.

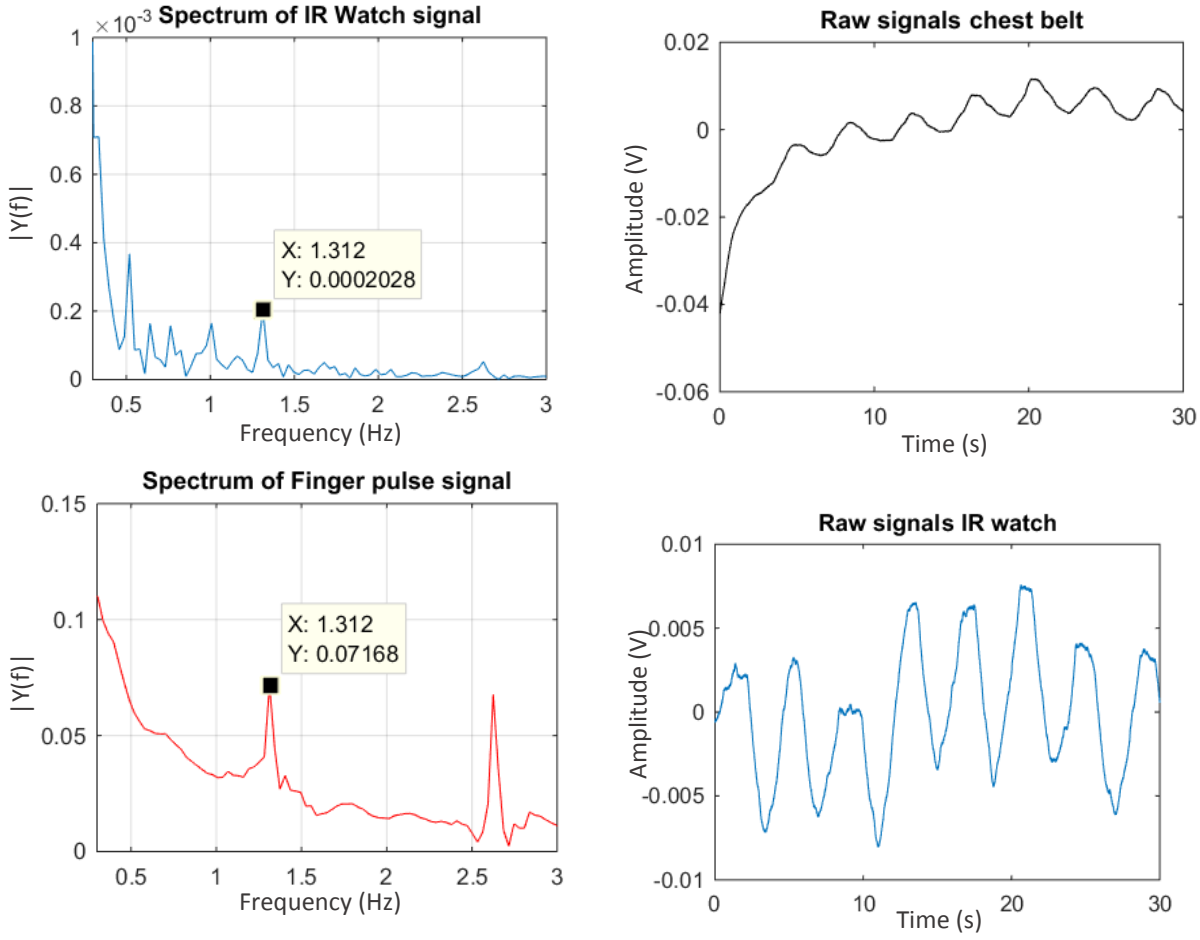

(a) (b)

Figure 4.12 Back chest measurement results with IR watch. (a) heart rate in frequency domain (b) respiratory rate in time domain.

4.2.3. Bio-impedance analyzer (BIA)

The bio-impedance analyzer (BIA) configured in direct conversion structure was used to measure respiration on five locations, including lower wrist, upper arm, front chest, side chest, back chest (see Figure 4.13). Reference signals were taken synchronously for heart rate and respiratory rate during each measurement. Each measurement lasts 30 seconds.

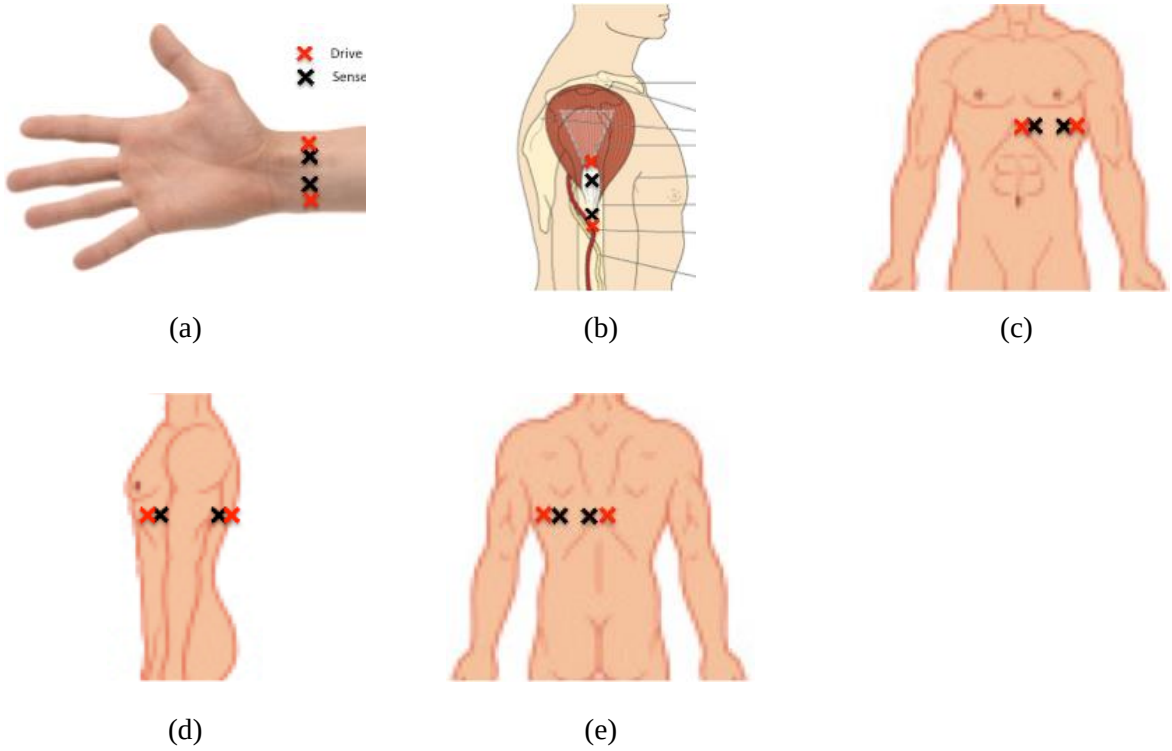

Figure 4.13 Tetrapolar configurations of bio-impedance analyzer for respiration and heartbeat measurement. (a) wrist lower, (b) upper arm, (c) chest front, (d) chest side, (e) chest back.

The summary of the respiration and heartbeat measurement results are illustrated in Fig. 4.14 – Fig. 4.18. Spectrum plots are used to reflect heart rate measurement, for which the strongest peak indicates the signal frequency. Time domain plots are used to demonstrate respiratory rate measurement, where vertical axes are measured signal amplitudes in voltage, and horizontal axes indicate time of the measurement in second. Detailed analysis on the measurement results are as follows.

To begin with, the sensitivity of BIA on measuring respiration varies among testing locations. The three locations on the chest are proven to be the most sensitive locations to detect clean respiration-related BIA signals. As indicated by Fig. 4.16 - Fig. 4.18, BIA signals captured at these locations have unbiased signals reflecting respiratory motion that match well with the references. Measurement results on upper arm for BIA show evident distortion over the 30-second measurement. However, approximating the most prominent peaks yield seven events, which

agrees with seven respirations measured by reference. Thus the respiratory rate can still be detected from upper arm. The BIA measurement in lower wrist could not pick up respiration signal.

The most reliable heart rate measurements by BIA were on lower wrist and front chest. The subject was breathing normally when doing the experiment. Frequency spectrum of BIA signals on upper arm and front chest are in good agreement with the finger pulse reference. We can also see a regular fluctuation from two time-domain plots of bio-impedance signal, which is very likely to be related to rhythmic breath.

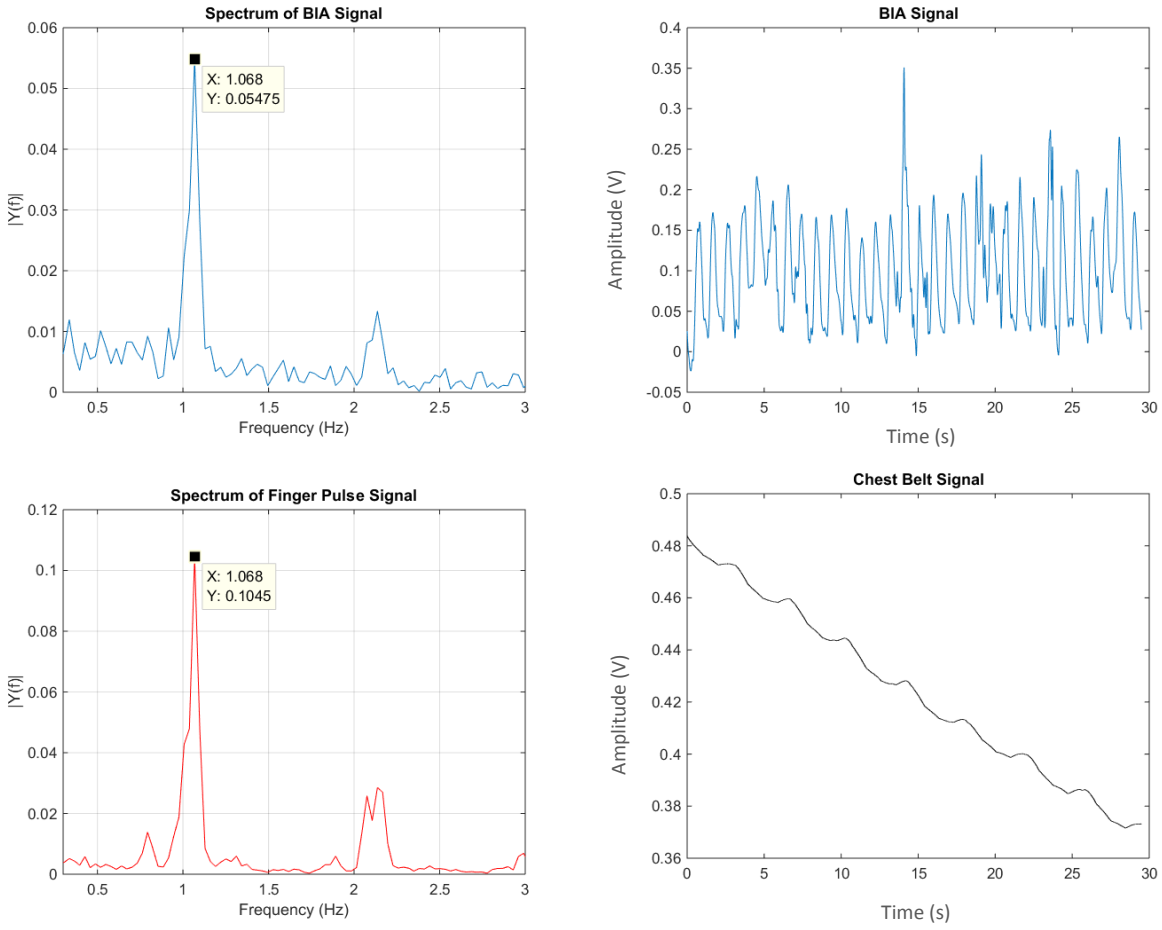

(a) (b)

Figure 4.14 Lower wrist measurement results with BIA. (a) heart rate in frequency domain (b) respiratory rate in time domain.

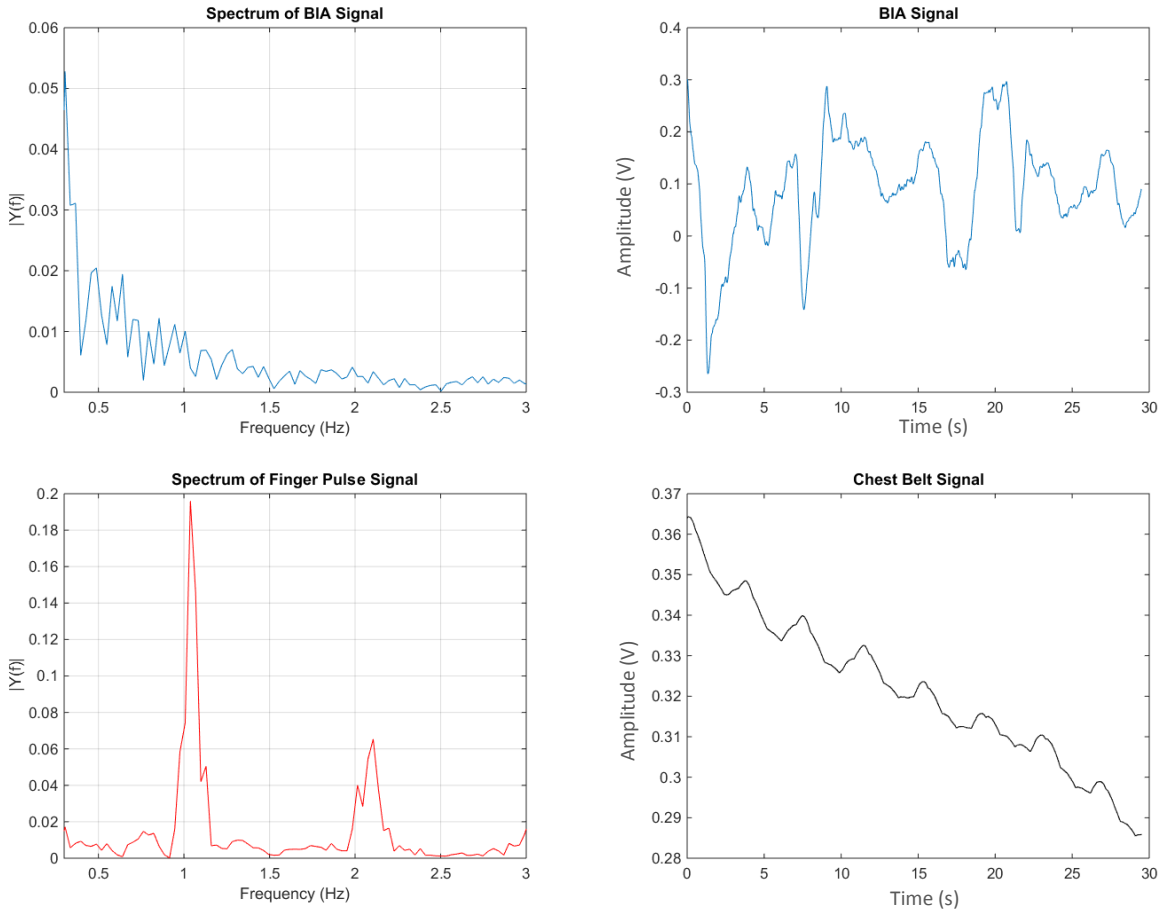

(a) (b)

Figure 4.15 Upper arm measurement results with BIA. (a) heart rate in frequency domain (b) respiratory rate in time domain.

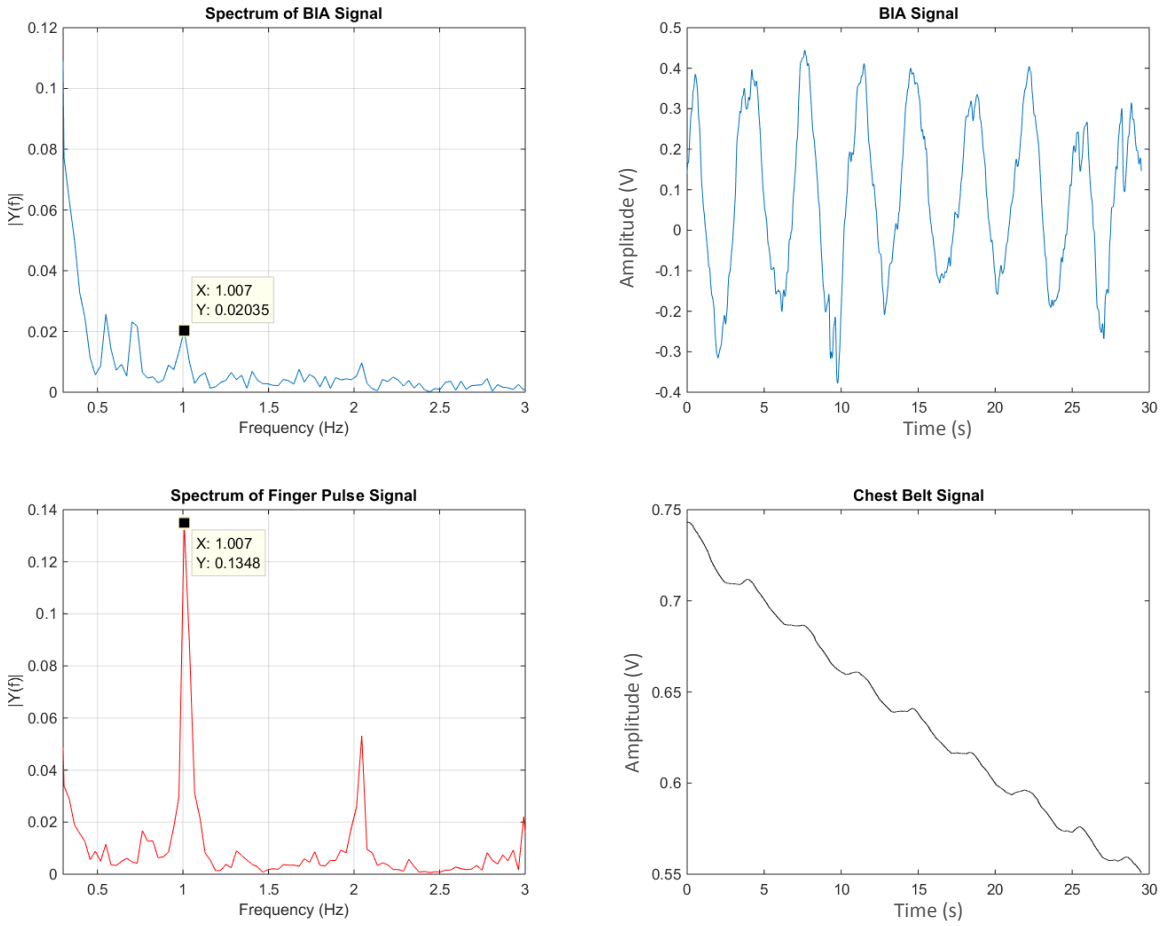

(a) (b)

Figure 4.16 Front chest measurement results with BIA. (a) heart rate in frequency domain (b) respiratory rate in time domain.

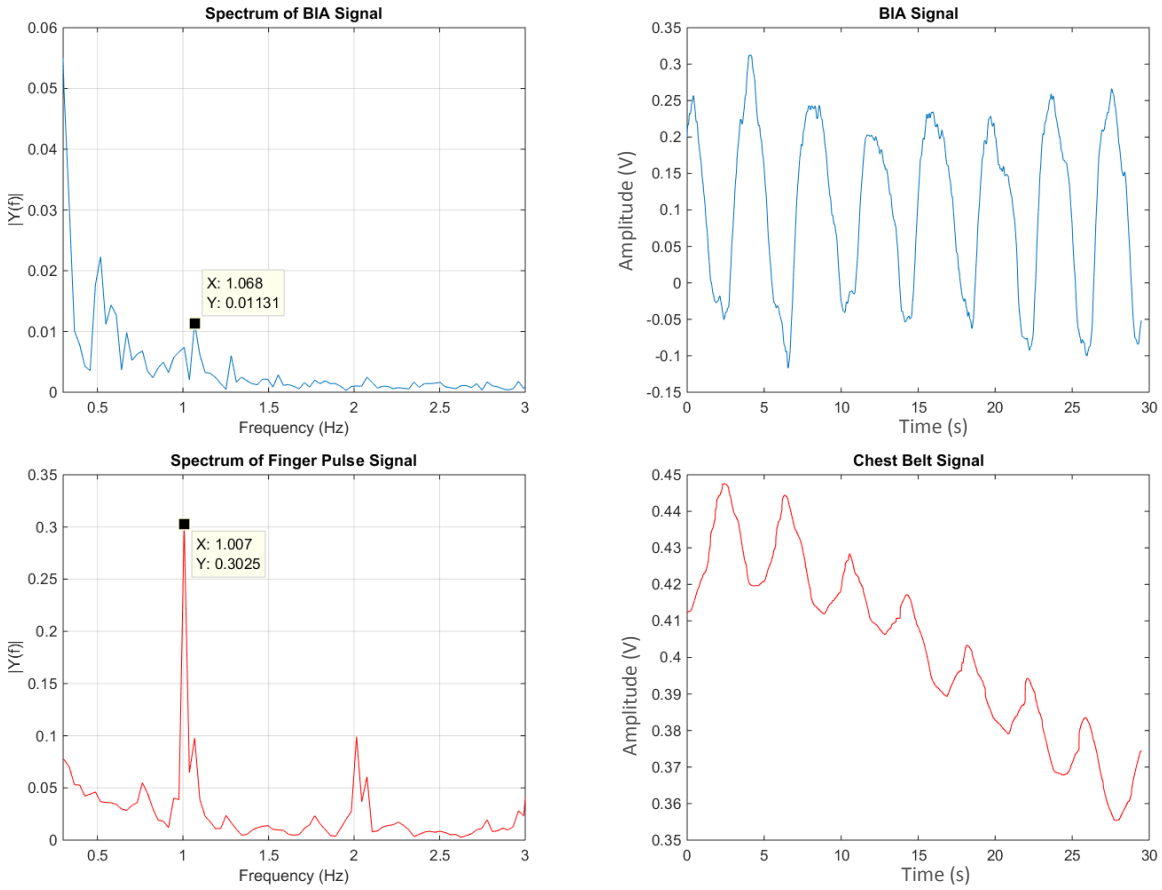

(a) (b)

Figure 4.17 Side chest measurement results with BIA. (a) heart rate in frequency domain (b) respiratory rate in time domain.

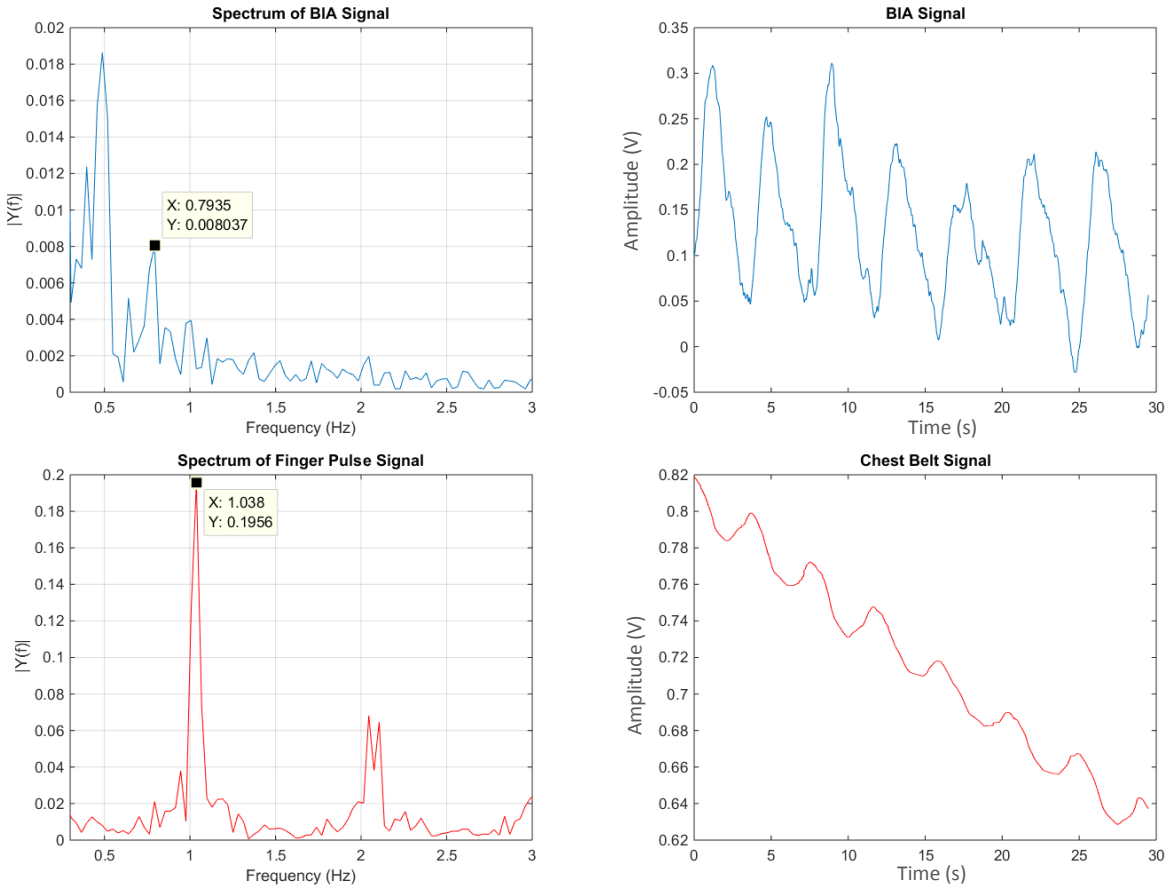

(a) (b)

Figure 4.18 Back chest measurement results with BIA. (a) heart rate in frequency domain (b) respiratory rate in time domain.

4.3. Summary

This chapter summarizes the performance of three bio-sensors, including ECG, infrared watch and bio-impedance analyzer, for heart rate and respiratory rate detection. Each sensor was tested in sync with a piezoelectric-based reference (chest belt for respiratory rate, whereas finger pulse transducer for heart rate). The performance on vital sign sensing for each sensor and detectable locations are listed in Table 4.3. Note that in Chapter 3.5 (Table 3.1) upper wrist was tested with BIA, which was able to detect heart rate. We have marked × for BIA heart rate detection on upper wrist.

Table 4.3 Heart rate and respiratory rate detectable location summary

Sensor Type	Vital Sign*	Detectable Locations					
		Lower Wrist	Upper Wrist	Upper Arm	Front Chest	Side Chest (Left)	Back Chest
ECG	HR			×	×	×	×
	RR						
Infrared Watch	HR	×	×	×			×
	RR	×	×	×	×	×	×
BIA	HR	×	×		×		
	RR			×	×	×	×

* HR = Heart rate, RR = Respiratory rate, X = detectable

The ECG with Biopac ECG100C module was proven to be reliable on locations around chest circumference and upper arm, whereas not able to pick up pulses from wrist or any respiratory signals. The captured heartbeat signals showed clear QPRS signatures and are relatively less sensitive to motion artifacts when measured on chest, while likely to be affected on upper arm. Though only 3 leads were used for sensing, the sticky resting electrodes and extended wiring

remain an issue that may cause skin irritation, mobility restriction and possible interference on physiological behavior patterns.

The infrared watch was the most capable candidate among the three tested biosensing techniques. The inbuilt commercial TI AFE4403 chip and infrared sensing unit can be configured for robust performance on measuring heart rate and respiratory rate. However, it is still susceptible to motion interferences and should be tested against a variety of scenarios among large population. The wrist watch design and removable infrared sensor evaluation module (EVM) offers potentials for wearable applications.

The BIA based monitoring system evaluated a novel method for vital sign sensing. It offers comparable heart rate readings to that of referencing finger pulse transducer and IR watch on the lower wrist, which presented the first BIA heartbeat monitoring system in the wristband configuration. Similar to IR watch, the BIA sensing system is also subject to motion artifact, and requires bulky instrumentations for signal conditioning. Thus a compact BIA platform with small form factor and robust signal conditioning algorithm is needed in future research.

Chapter 5. Continuous-wave Radar for Physiological Monitoring

5.1. Doppler radar measurement system

5.1.1. Measurement Principle

By the principle of Doppler Effect, when a target is moving radially (either toward or away from the transmitter), a radio signal that bounces off the surface of the moving target will carry a Doppler shift in the backscattered signal. The shift is reflected in form of a frequency difference between the transmitting signal and echo. This component is expressed as [76]:

$$f_d = \frac{2 f_t v_r}{c} \tag{5.1}$$

where

f_d is the Doppler frequency carried in echo signal in Hz

f_t is the frequency of the transmitting signal in Hz

v_r is the radial velocity of the moving target in m/s

c is the speed of light (300,000km/s), which is also the speed of radio wave through air

Since the wavelength of the transmitter carrier signal is

$$\lambda = \frac{c}{f_t} \tag{5.2}$$

thus (5.1) can be rewritten as

$$f_d = \frac{2 v_r}{\lambda} \tag{5.3}$$

From (5.3), we know that from the Doppler frequency shift in echo signal and wavelength of the transmitting signal, radial velocity of the moving target can be measured. If f_d is integrated over time, while ignoring the constant term of integration, the instantaneous phase variation $\theta(t)$ can be expressed as

$$\theta(t) = 2\pi \int f_d(t) d(t) = 2\pi \int \frac{2v_r}{\lambda_t} d(t) = \frac{4\pi x(t)}{\lambda_t} \tag{5.4}$$

where $x(t)$ is the time varying displacement of the moving target. From (5.4), it indicates that the displacement of the moving target is also accessible by extracting the time varying phase component (Doppler phase shift) from the echo signal. In theory, any physiological displacement can thus be estimated by demodulating the Doppler phase shift from the echo signal.

5.1.2. Doppler Radar Fundamentals

5.1.2.1. CW Quadrature radar

In general, cardiopulmonary activities create periodic changes on chest wall, such minute motions can be detected by Doppler radar in a form of phase modulation in echo signals.

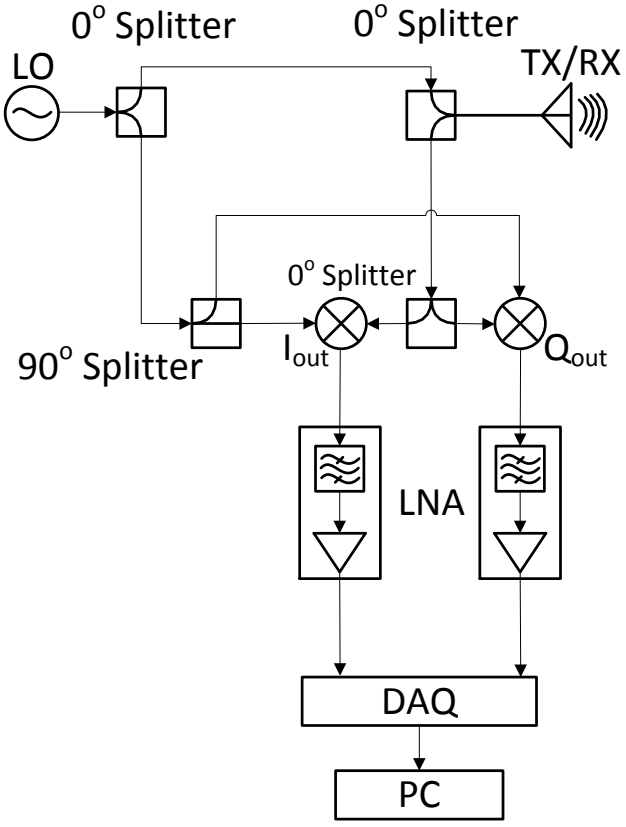

Figure 5.1 Architecture of CW Quadrature Doppler radar

To demodulate rate information from baseband signals, single channel radar receiver is sufficient because phase changes are proportional to amplitude variation of the reflected signal [62][63]. If accurate displacement over time is to be assessed, quadrature radar receiver is needed. Both in-phase/quadrature-phase (I/Q) outputs are processed concurrently to demodulate phase information, which can be used to recover displacement in time domain.

Figure 5.1 shows the architecture of a continuous-wave (CW) quadrature Doppler radar. The signal source, or the local oscillator (LO), generates a single tone signal continuously. It can be represented as a sinusoid of carrier frequency *f*, shown as

$$T(t) = A_T \cos(2\pi ft + \Phi(t)) \tag{5.5}$$

or

$$T(t) = A_T \cos(\omega t + \Phi(t)) \tag{5.6}$$

where A_T is the amplitude of transmitting signal in voltage, $\Phi(t)$ is the phase noise inherent to the local oscillator, $\omega = 2\pi f$ is the angular frequency in radian. It then goes through a passive component 0° splitter, which splits the transmitting signal into two identical half-the-power components. One of the divided signal is sent to the summing port of a 0° splitter, routed to the TX/RX antenna and radiated through the air. When a moving target intercepts the propagating signal at distance d_0, a portion of the transmitting signal will be reflected immediately. The backscattered signal *R(t)* carries a Doppler phase shift associated to the time-varying motion of the target, which is represented in a displacement function over time *x(t)*. The total distance between TX/RX antenna and the moving target is relevant to time.

$$d(t) = d_0 + x(t) \tag{5.7}$$

It is necessary to consider time delay of the propagation between the antenna and the target, which is basically the time cost for transmitting signal to reach surface of the moving target. At the time of reflection, the actual distance is modified as

$$d(t - \frac{d(t)}{c}) = d_0 + x(t - \frac{d(t)}{c}). \tag{5.8}$$

Thus the round-trip time cost during the propagation is

$$t_d = \frac{2(d_0 + x(t - \frac{d(t)}{c}))}{c} \tag{5.9}$$

Backscattered signal R(t) can be expressed as

$$R(t) = A_R \cos(\omega(t - t_d) + \Phi(t - t_d) + \theta_0) \tag{5.10}$$

where θ_0 is constant phase shift associated with the distance between radar and the target.

Considering the other divided part of the LO signal in Figure 5.1, when delivered to a 90° splitter it is branched up into in-phase and quadrature-phase (90°) components. The I channel signal takes the same format as (5.6), while the Q channel signal has a 90° phase difference. I/Q signals can thus be represented as

$$I(t) = A_T \cos(\omega t + \Phi(t))$$
$$Q(t) = A_T \sin(\omega t + \Phi(t)) \tag{5.11}$$

They are then fed to two passive mixers individually, and each mixed with half of the backscattered signal *R(t)* to generated down-converted baseband signals. Taking *I(t)* as an example, in the mixer, *I(t)* and *R(t)* are multiplied as

$$\begin{aligned} \mathrm{I}_{out}(t) &= I(t) * R(t) \\ &= \frac{1}{2} A_T A_R [\cos(2\omega t - \omega t_d + \Phi(t) + \Phi(t - t_d) + \theta_0) \\ &\quad + \cos(\omega t_d + \Phi(t) - \Phi(t - t_d) - \theta_0)] \end{aligned} \tag{5.12}$$

Following the output port of the mixer, a low-pass filter will remove the term with double carrier frequency ($2\omega t$), leaving the baseband signal of interest $B_I(t)$ as

$$B_I(t) = \frac{1}{2} A_T A_R \cos(\omega t_d + \Phi(t) - \Phi(t - t_d) - \theta_0) \tag{5.13}$$

Substituting (5.9) into (5.13), I channel baseband signal can be rewritten as

$$B_I(t) = \frac{1}{2} A_T A_R \cos[\frac{2\omega d_0}{c} + \frac{2\omega * x(t - \frac{d(t)}{c})}{c} + \Phi(t) - \Phi(t - \frac{2d_0}{c} - \frac{2x(t - \frac{d(t)}{c})}{c}) - \theta_0] \tag{5.14}$$

Assume the term $\frac{2x(t - \frac{d(t)}{c})}{c}$ in phase noise is negligible as $x(t) << d_0$, and the term $\frac{d(t)}{c}$ can be approximated to zero so that $x(t - \frac{d(t)}{c}) \approx x(t)$ [77]. (5.14) is then modified as

$$B_I(t) = A_I \cos[\frac{4\pi x(t)}{\lambda} + \Delta\Phi(t) + \theta] \tag{5.15}$$

where

$A_B = \frac{1}{2} A_T A_R$ is the amplitude of the baseband signal in channel I,

$\frac{4\pi x(t)}{\lambda}$ is the Doppler phase shift modulated from *x(t)*,

$\Delta\Phi(t) = \Phi(t) - \Phi(t - \frac{2d_0}{c})$ is residual phase noise,

$\theta = \frac{2\omega d_0}{c} - \theta_0$ is the total constant phase shift due to the distance between target and radar.

Under similar deduction, baseband signal in Q channel can be obtained as

$$B_Q(t) = A_Q \sin[\frac{4\pi x(t)}{\lambda} + \Delta\Phi(t) + \theta] \tag{5.16}$$

The I/Q channel signals will be amplified, sampled in data-acquisition system (DAQ), and sent to PC for processing.

5.1.2.2. Displacement estimation

As shown in (5.15)(5.16), Quadrature radar outputs of I/Q channels contain the same Doppler shift, which transcribe an arc when they are plotted as (I + i*Q) in complex plane (see Figure 5.2). When the arc center is located on the origin of the complex plane, arctangent function can be used to demodulate phase shift [64][65][66].

$$\varphi = \frac{A_Q}{A_I} \arctan(\frac{4\pi x(t)}{\lambda} + \Delta\Phi(t) + \theta) \tag{5.17}$$

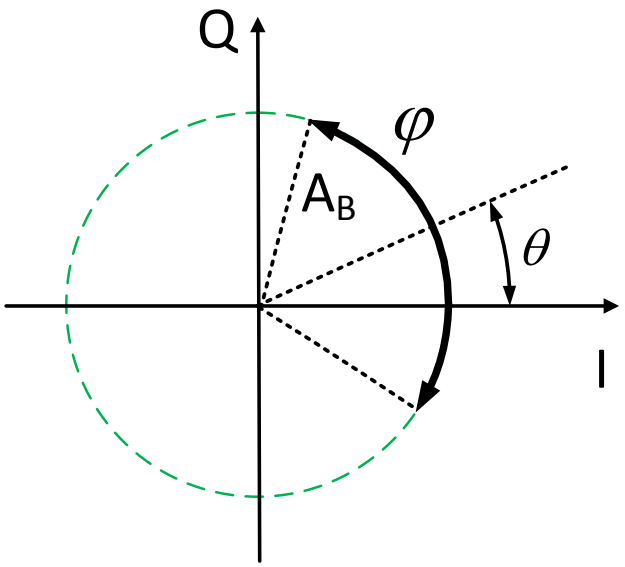

Figure 5.2 Complex plane demonstration of I/Q channel baseband signal transcribing an arc (AB represents baseband signal amplitude)

When there's no amplitude imbalance between channels, the amplitude of I/Q channel outputs should be the same. Assume residual phase noise can be ignored, and total constant phase θ can be eliminated by arc rotation, the arctangent function will yield the following term

$$\tilde{\varphi} = \frac{4\pi x(t)}{\lambda} \tag{5.18}$$

Displacement function over time *x(t)* can thus be extracted by

$$x(t) = \frac{\tilde{\varphi} \cdot \lambda}{4\pi} \tag{5.19}$$

5.1.2.3. Demodulation challenges

In actual measurement, however, inherent dc offset commonly exist in both channels due to stationary target reflection, LO chain leakage and RF chain reflection [78]. The expressions of baseband I/Q signals are then modified as

$$B_I(t) = V_I + A_B \cos(\frac{4\pi x(t)}{\lambda} + \Delta\Phi(t) + \theta)$$
$$B_Q(t) = V_Q + A_B \sin(\frac{4\pi x(t)}{\lambda} + \Delta\Phi(t) + \theta) \quad (5.20)$$

where V_I and V_Q are dc offsets associated with I and Q channel. An illustration of IQ formed arc with dc offset is shown in Figure 5.3.

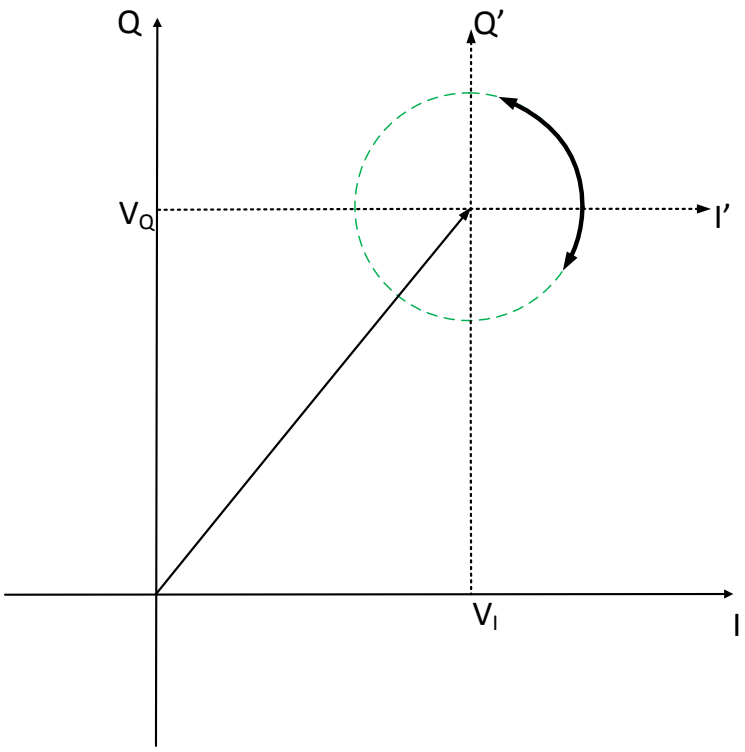

Figure 5.3 Arc with dc offset

Center estimation is performed in order to put arc center back to the origin of the complex plane for arctangent demodulation [79]. The aim of using this method is to find the correct center of the arc so that it can be tracked back to origin of the complex plane.

Since cardiac pulse induced movement on the body surface is at sub-millimeter level, its associated phase shift at carrier frequency of 2.4GHz is only a few degrees. The limitation of arc length imposes another challenge of accurately recovering arc center based on above method,

which may cause ambiguity and error in estimation. Thus radius correction [72] is adopted to calibrate radar data. It can estimate the correct center of a short arc by using the radius of a longer arc transcribed from a larger displacement of the same target. To satisfy this theory, the target has to be carefully aligned in line-of-sight to the antenna probing direction, and placed in far-field region.

During center estimation, when arc center is tracked back to origin, its radius is obtained by finding its crossing point on the I-axis, as shown in Figure 5.4. Due to the fact that arc radius A_B is essentially the amplitude of I/Q channel baseband signals, it correlates to received power level. In theory, if a target is measured under same measurement settings in the far field, estimated radius originated from a larger motion would be the same as that of a shorter motion. In other words, a short arc's correct radius is indirectly accessible by estimating the radius from the longer arc generated by the same target in a larger motion (see Figure 5.5). Detailed procedure of radius correction can be found in [72].

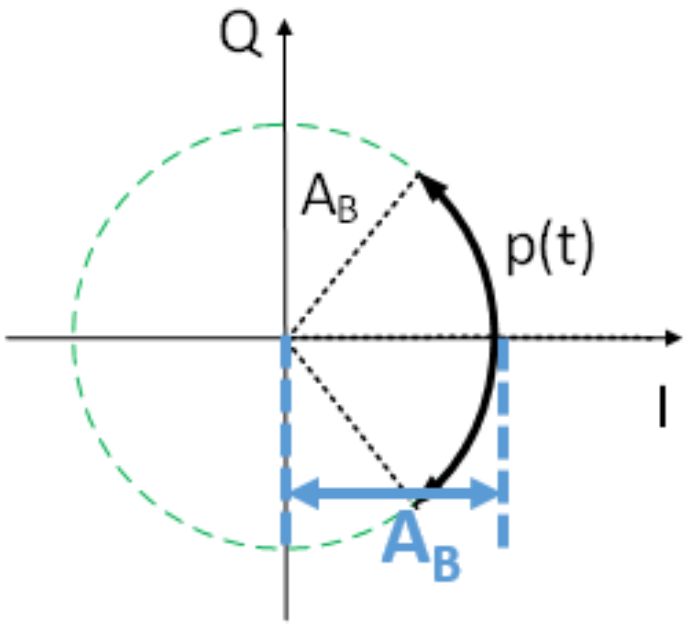

Figure 5.4 Finding arc radius

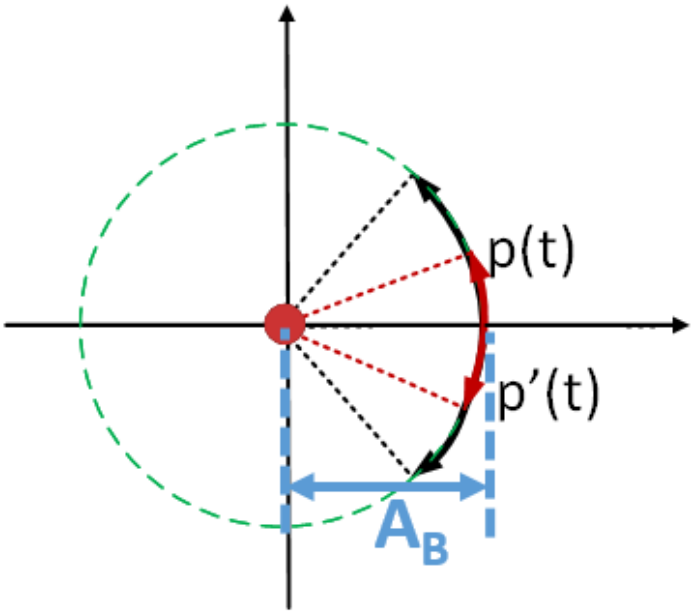

Figure 5.5 Long arc and short arc sharing the same radius

As described in [65][70], quadrature channel imbalances (phase/amplitude imbalances) often cause signal distortion and estimation error. Nonetheless, the phase changes discussed in this work are very small, imbalance distortion on the transcribed arc can be neglected.

5.1.3. Summary

This chapter discusses the fundamentals of Doppler radar measurement. Mathematical deduction on how displacement information can be estimated using CW quadrature Doppler radar transceiver was presented. During the process of radar signal propagation and demodulation, several factors got involved including dc offset, limited phase angle and channel imbalance, which poses challenges in the estimation. Radius correction was adopted to calibrate center estimation process, in which correct radius information associated with data of interest should be determined in the first place. Experimental evaluation of the calibration method on sub-millimeter displacement measurement will be presented in the following chapter.

5.2. Doppler Radar Sub-Millimeter Physiological Displacement Estimation

5.2.1. Experiment set-up

This chapter presents the estimation of sub-millimeter displacement by measuring a programmable mechanical mover that outputs a series of sinusoidal movements. They range from 0.1mm to 1mm at an oscillation frequency of 1Hz, which represent heartbeat activity induced displacements on the surface of the body. An infrared camera based motion tracking system is also used to synchronously measure the same motions, with a reported accuracy on the order of 10μm. The results indicate the feasibility of estimating displacement of heart motion on chest wall using quadrature Doppler radar with high accuracy.

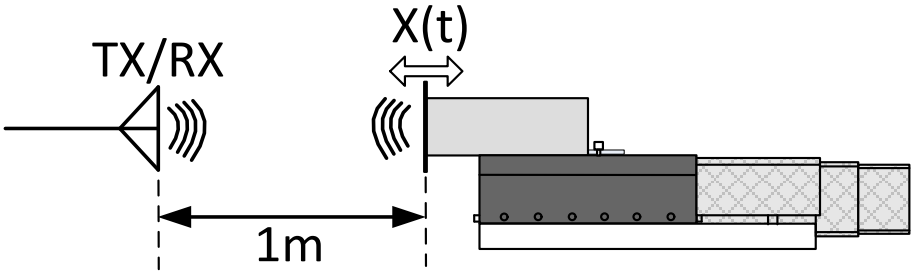

Figure 5.6 Linear stage displacement measurement

Figure 5.6 demonstrates the measurement on a mechanical phantom emulating chest motion. The TX/RX antenna is part of the CW Quadrature Doppler radar system shown in Figure 5.1. It was operated at 2.4GHz with an output power of 10dBm. It is composed of an ASPPT 2988 patch antenna used for both transmitting and receiving (TX/RX) signals, three ZFSC-2-2500 0°splitters, one ZX10Q-2-25-S+ 90° splitter, and two ZFM-4212+ mixers. The quadrature receiver outputs were fed to Stanford SR560 LNA for DC coupling, low-pass filtering and amplification. The cutoff frequency of the filter was set to 3Hz to eliminate noises from hardware and stationary object reflection. After A/D sampling, the raw data will be stored through LabVIEW in PC and processed in Matlab.

The moving target is carefully aligned with the antenna at 1 meter distance, which is located in the far field. A Griffin Motion MLS series linear stage is used for simulating chest wall

movement, which is able to output fine periodic motions with an accuracy of 4μm. It varies in displacements to cover a spectrum of possible heart activities.

An Advanced Realtime Tracking (ARTrack) System composed of a pair of infrared cameras was used for reference. It is capable of capturing three-dimensional coordinates of a retro-reflective marker, of which y-axis data were computed for superior-posterior motion displacement. To track target motion, the marker is attached to the center point of the measured target surface. The data from reference system and radar system were synchronously obtained. It is achieved by feeding the internal sync signal from camera data acquisition platform to DAQ to be concurrently digitized with radar analog outputs. It is crucial to include these set of data for it serves to validate the real outputs of linear stage.

Figure 5.7 shows the experimental set-up configuration, with radar placed in the mid-point between camera pairs, and linear stage located at line-of-sight of TX/RX antenna's probing direction. Linear stage mounts a metallic plate as the target of interest for both sensing systems. It is placed at a spot where infrared rays from camera pairs formulate a right angle for best tracking performance.

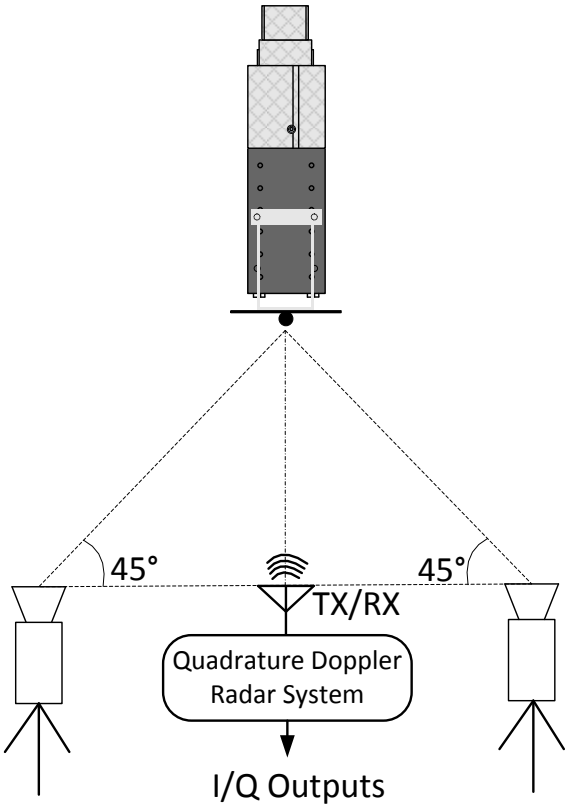

Figure 5.7 Experimental set-up configuration of quadrature Doppler radar, ARTrack infrared camera system, and linear stage.

5.2.2. Measurement results and discussions

Linear stage was programmed to perform sinusoidal motions with fixed frequency of 1Hz and varied displacements ranging from 0.1mm to 1.0mm, in order to emulate cardiac pulse displacement on the body surface. For each displacement, the measurement was repeated 3 times, for 60 seconds each with a sampling frequency of 1000Hz. Their results were averaged to yield final estimations. When processing measured radar data in Matlab, an FIR low-pass filter with cutoff frequency of 5Hz was used to remove clutter noise. Then the filtered radar data were corrected using radius correction method mentioned in Section 5.1.2.3 for accurate displacement estimation. The estimated radius is 1.118V, which is acquired from a sinusoidal motion of metallic plate with displacement of 40mm and frequency of 0.3Hz. This radius was made equal to that of the shorter arcs.

Table 5.1 shows a comparison of displacement measurement results between radar system and reference infrared cameras. Absolute error in μm is defined as the difference between measured value and the nominal one. Relative error evaluates the severity of error in estimation, which is defined as absolute error over nominal value. Values listed here are averages from the three repeated measurements.

Table 5.1 Comparison of displacement measurement results

Nominal Displacement (mm)	**Radar Measurement**				**Camera Measurement**			
	Standard Deviation (μm)	***Estimated Displacement Ave. (mm)***	***Absolute Error (μm)***	***Relative Error***	***Standard Deviation (μm)***	***Estimated Displacement Ave. (mm)***	***Absolute Error (μm)***	***Relative Error***
1.0	1.87	0.992	7.81	0.78%	2.69	1.037	37.28	3.73%
0.9	2.08	0.898	2.44	0.27%	1.06	0.941	40.67	4.52%
0.8	0.30	0.801	1.03	0.13%	1.17	0.838	38.44	4.80%
0.7	2.83	0.704	4.00	0.57%	0.40	0.739	39.48	5.64%
0.6	2.81	0.607	7.47	1.24%	10.93	0.629	29.06	4.84%
0.5	2.98	0.507	6.72	1.34%	4.39	0.524	24.33	4.87%
0.4	1.42	0.407	6.86	1.72%	1.21	0.423	22.87	5.72%
0.3	1.85	0.307	6.99	2.33%	5.97	0.332	31.96	10.65%
0.2	0.38	0.205	4.52	2.26%	0.90	0.238	37.73	18.86%
0.1	2.03	0.096	3.88	3.88%	0.56	0.136	35.52	35.52%

Measurement results in displacement for two systems are plotted in Figure 5.8. Radar measurement results show a good agreement with its nominal values, while camera system presents an overestimation throughout all measurements. Detailed analysis on measurement accuracy is as follows.

To start with, standard deviation of repeated measurements evaluates the performance of each system. It is scaled in unit of μm to better reflect how much variation each measurement differs from the average. As shown in Figure 5.9, both systems show good repeatability in that their deviations over three measurements are no more than 6μm for displacements within 1000μm, except for 0.6mm measurement of camera system.

In Figure 5.10, a clear distinction of absolute errors between radar and camera measurement shows that radar system has superior estimation accuracy. Similar comparison was demonstrated

in Figure 5.11, showing less than 5% error rate was achieved by radar measurement. However, both systems have their limitations in maintaining accuracy when nominal displacement continues to decrease, as the estimation error begins to intensify. For radar measurements, if nominal displacement value decreases by 10 times, relative estimation error increases by 5 times. However, it gets worse for camera measurements, because the associated increase in relative error is double of its counterpart. By comparing only the absolute errors in measured displacements, radar measurement has well maintained its results under 10μm, while those of the camera estimations range from 20μm to 40μm.

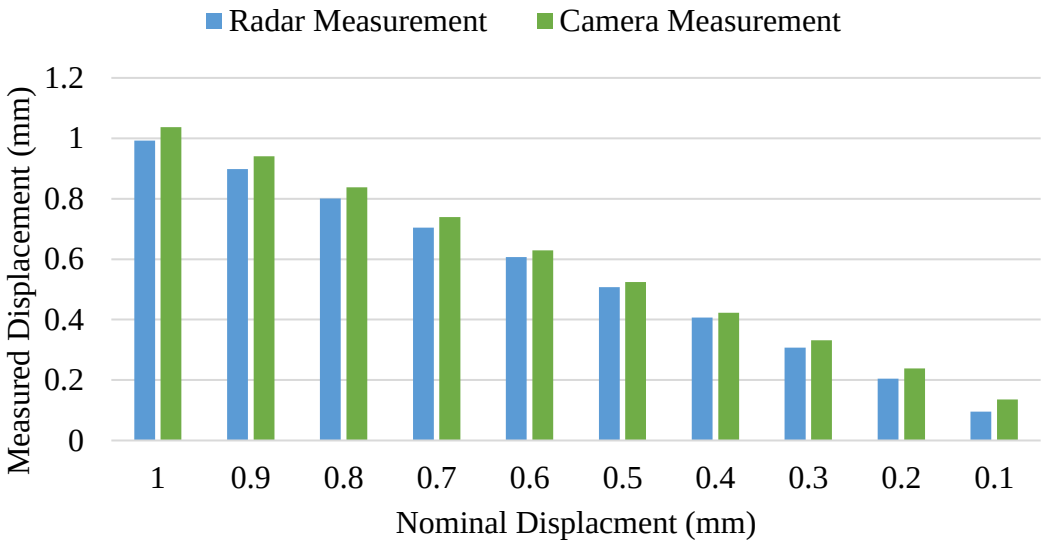

Figure 5.8 Measured displacement comparison

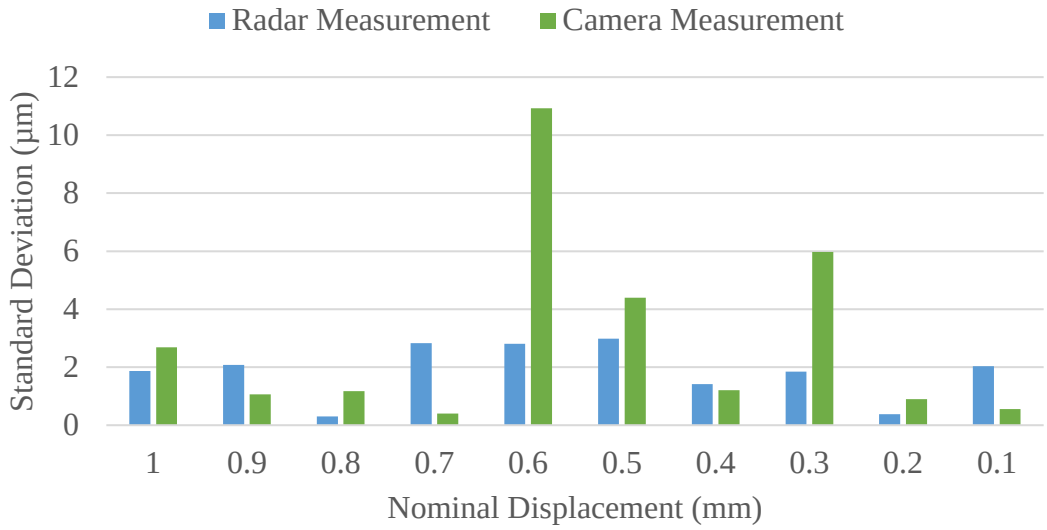

Figure 5.9 Standard deviation comparison

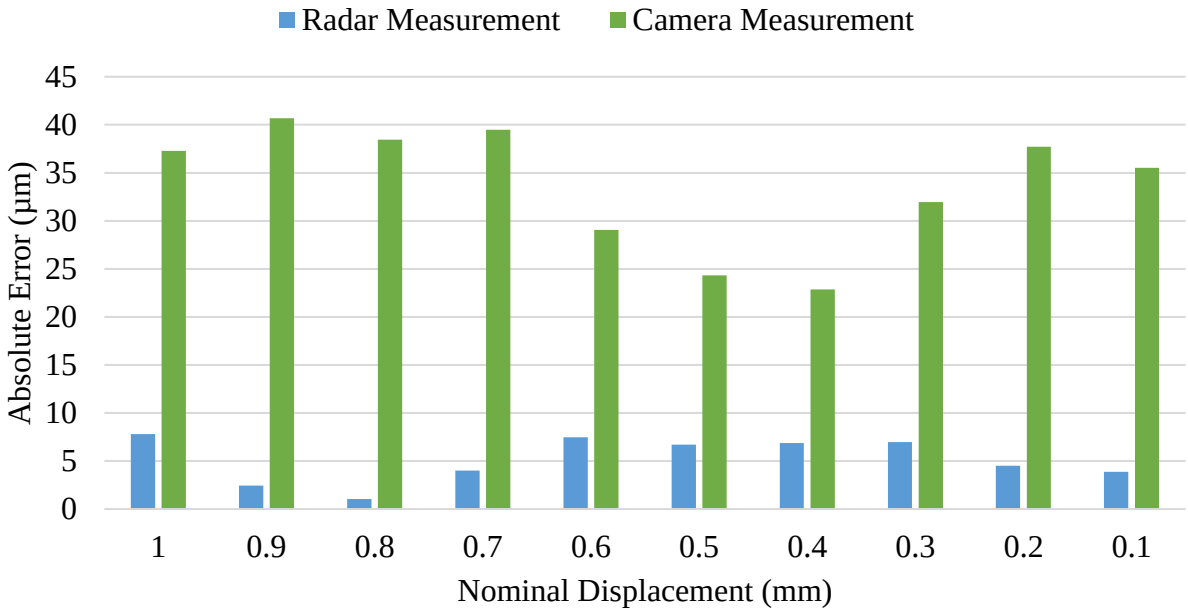

Figure 5.10 Absolute error comparison

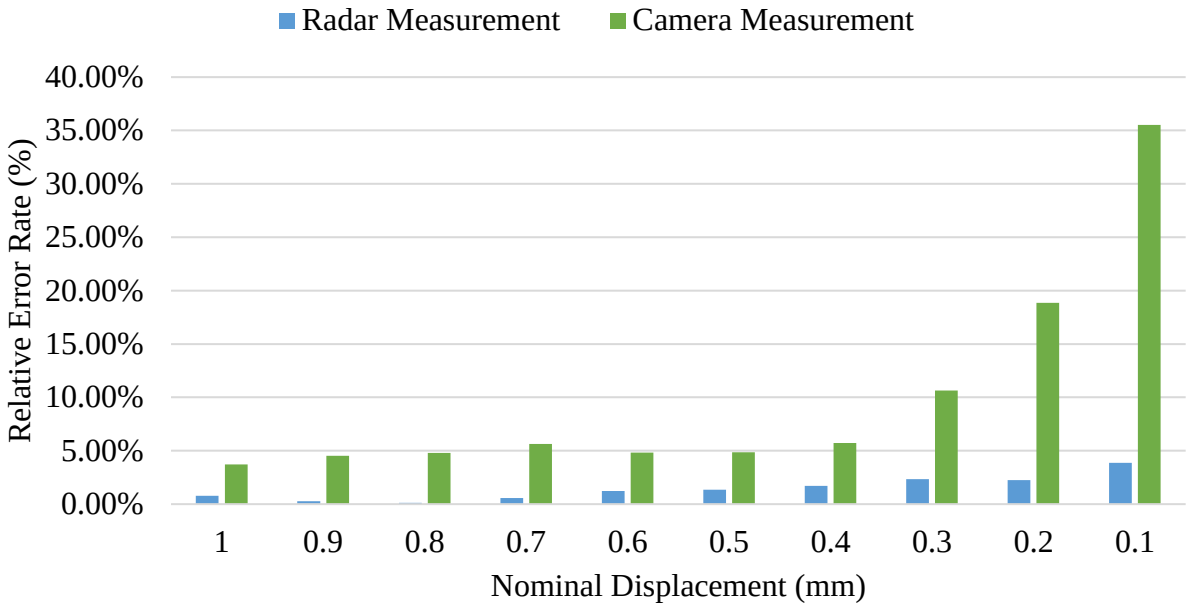

Figure 5.11 Relative error comparison

Time domain displacement plots of 1.0mm and 0.3mm estimation are selected as examples, and plotted in Figure 5.12. Linear stage output is simulated in Matlab and plotted as red dotted line. It is a sinusoid of frequency at 1Hz. Camera estimation of y-axis coordinates over time are adjusted to make their mean at zero, plotted as dashed line in black. Blue solid line represents the radar-recovered displacement variations. It can be seen that for 1.0mm case, both radar trace and camera trace fit closely with the reference. Peak detection results reveal that negative peaks of radar measured displacement don't quite overlap with simulation at the beginning of the measurement, so does camera estimation. And for 0.3mm case, camera measured displacement trace carries spikes in some of its peaks as shown in Figure 5.12(b), causing unwanted overestimation errors. As indicated in Table 5.1, Doppler radar measurements achieve higher accuracy.

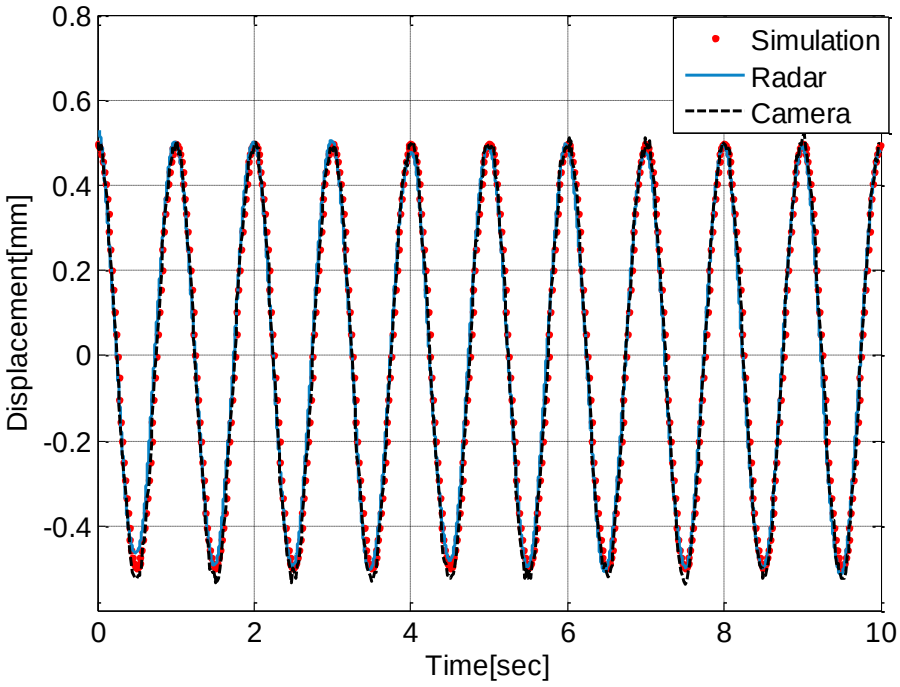

(a)

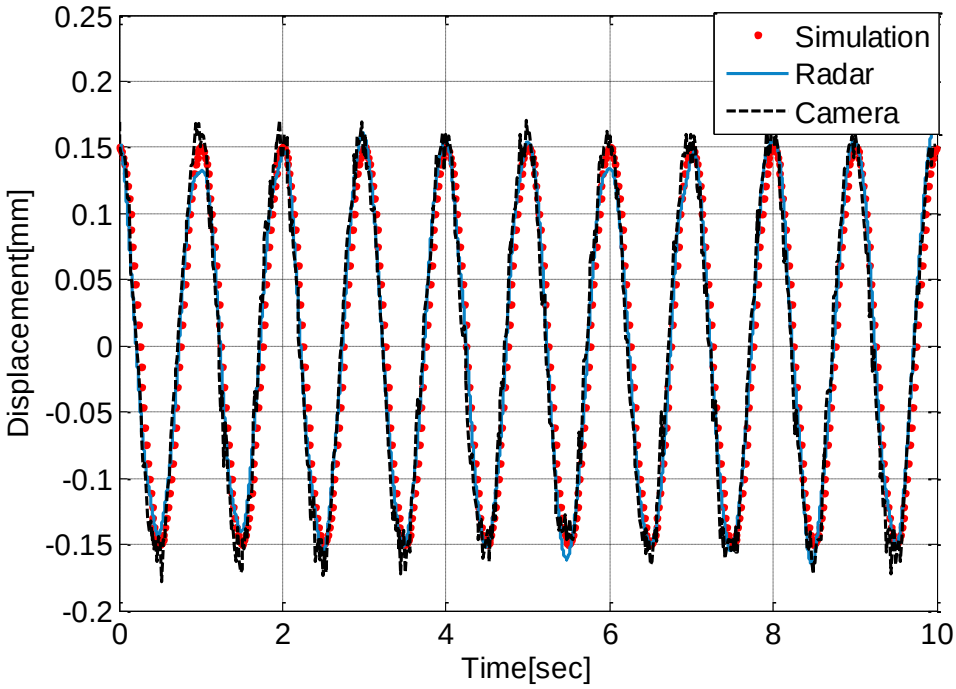

(b)

Figure 5.12 Time domain comparison of (a) 1.0mm displacement and (b) 0.3mm displacement estimations with reference. Dotted line is computer simulation of standard sinusoid with same

displacement and 1Hz frequency, which represents the output of linear stage. Solid line is the reconstructed displacement measured by radar. Dash line stands for camera results.

5.2.3. Summary

This chapter discusses the feasibility of measuring sub-millimeter displacement with Doppler radar with high accuracy. An infrared camera motion tracking system is employed for comparison. Measurements took place on the target displacements of one or only fractions of a millimeter. Quantitative results were compared, as well as reconstructed time domain displacement traces. Overall, although infrared camera was used initially as a reference, Doppler radar system performance is superior for all the measurements.

Chapter 6. Conclusion

6.1. Challenges

Physiological monitoring systems monitors vital sign parameters for health condition prognosis and diagnosis. These systems extract weak physiological signals from human subjects via transducers that are conditioned by various signal processing techniques. The challenges lie in the difficulties of acquiring the signals at full strength over the optimum position. Both contact and non-contact methods have shown adequacy in obtaining heart rate and respiration rate with sufficient accuracy when compared with gold standards. This thesis aimed to tackle the hurdle of acquiring the weak physiological parameters accurately via novel instrumentation and signal processing techniques.

6.2. Summary

In this thesis, a BIA based heart rate sensing method was proposed. Under direct conversion architecture, the system was able to detect very weak pulse-related impedance changes over the wrist via four electrodes, which matches well beat-to-beat measurement results from finger pulse transducer. Such a configuration confines a wristband design, which has potential application merits in wearable heart beat sensor.

A comprehensive comparison was also provided in this work, which covers a wide range of biosensors for heart rate and respiration rate sensing over conventional and non-conventional locations. Extensive data collection and analysis provided in-depth understanding of each biosensor's performance and offered insights in implementation in vital sign monitoring wearable devices.

Quadrature Doppler radar displacement estimation is of interests in non-invasive physiological sensing. It was proposed to detect small displacements on the body surface resulting from cardiac

activities. Incorporated with radius correction method, fine motion created by a linear mover with sub-millimeter displacements can be accurately measured without ambiguity. The accuracies for 0.1mm – 1mm measurements were maintained on the same order, and an error rate within the range of 0.13% and 3.88%. Such technique could serve as an approach for high accuracy torso displacement measurement, and potentially be applied to cardiopulmonary motion pattern tracking and pulse pressure monitoring. The lead-free feature of radar sensor eliminates any wiring configuration to the subject, and is a good candidate of non-contact physiological monitoring.

6.3.Future work

Future work of the thesis research will be focused on the feasibility of implementing BIA vital sign sensing on a wearable, the consideration of improving physiological signal quality, and novel calibration methods for Doppler radar displacement estimation. They can be categorized into following tracks:

- A BIA sensing unit will be developed, including part selection, schematic and layout design, fabrication and assembly. Extensive debugging and parts selection are needed to increase the stability of the measurement and minimize the board form factor. The consideration of acquiring more reliable data from large population of human subjects will be taken into account. The performance of other types of electrodes will be studied and evaluated in the future.
- Since physiological monitoring with contact or non-contact sensors commonly face motion artifacts due to unwanted and unpredictable body motions. A cancellation technique will be sought in order to implement an algorithm in the hardware or signal processing.
- Novel radius correction method for reliable center estimation without using linear stage. Since using linear stage as a calibration tool is not always possible in practical application, by shifting the radar antenna incrementally at a few stops could essentially create additional data points. It offers an alternative solution for small motion recovery, which can be used for torso displacement estimation.

- Since IR watch and BIA are good candidates in optimum location sensing measurement, it is promising to develop arm-based wearable device that can extract respiration rate without using respiratory chest belt.

Appendix A. Bio-impedance Analysis Human Testing Protocol

A.1. CHS #19176 Research Protocol

Title of Project: **Respiratory Effort Sensing and Harvesting**

Principal Investigator: Olga Boric-Lubecke; Ph.D.; Electrical Engineering Department

Co-Principal Investigator: Jia Xu; Electrical Engineering Department

Abstract

Unobtrusive sensing of respiratory effort and heartbeat can be valuable for continuous medical monitoring. Our research group is developing low-cost zero-net energy wearable biosensors for unobtrusive, continuous, respiratory effort and heart beat sensing and harvesting. The goal is to produce self-powered unobtrusive sensors suitable for continues (24/7) health monitoring. The advantages of this technique is that first; the patient is not wired to monitoring equipment, and second; there is no battery to be replaced or disposed. A large sample of human subjects is needed to better understand how variations in the population affect the performance of our biosensors. The objectives of our project and the proposed experiment methods on human subjects are elaborated below.

1. Specific Aims

The objectives of this project are to develop and implement zero-net energy wearable biosensors that can sense and harvest energy from respiratory effort. The goal is to produce self-powered unobtrusive sensors suitable for continuous (24/7), unobtrusive health monitoring. Our system consists of three components, 1) physiological sensing/harvesting module, 2) local module that will condition and store harvested potentials, and extract physiological data, and communicate this information to the third part of the system which is 3) a remote module, via a short range, low data rate wireless link.

However, a good understanding of how variations in the population affect the performance of our systems is needed, thus we propose to conduct human testing for better understanding and improvement of our works. The experiment requires a human subject wearing a shirt with our embedded system. The system detects his/her respiratory rhythm and heart beat data and harvests the energy from his/her breathing and heart beat. Then the harvested energy will be conditioned and stored to be distributed to other parts of the system when needed and sends the physiological data to the wireless link. Wireless link then collects the data and sends it via a low data rate wireless link to a remote computer to be further processed and analyzed. Each experiment will be done in a human performance laboratory and is expected to be two one-hour sessions.

2. Background and Significance

Human energy harvesting for wearable and portable electronics was proposed in the mid 1990's [1]. While a number of potential human energy sources were identified in [1], human energy harvesting has mostly been focused on kinetic energy [2-4], and more recently on thermal energy [5]. Primary self-powered electronic devices have included self winding wrist watches and more recently laptops with hand cranks and foot pedals [1-2]. The recent efforts to scavenge human kinetic energy using piezoelectric sensors and electromagnetic generators placed in shoes, and backpacks with spring-loaded straps have shown promise [2-3]. Also it has been demonstrated that electromagnetic scavenging is more efficient than piezoelectric [3, 6].

Perhaps the most readily available form of human power is respiration, yet no significant work has been done on energy harvesting from movement of the chest walls due to respiratory effort. Similarly, human electrical signals have been identified as a potential energy source [1, 7], with no published efforts to date. On the other hand; wearable biosensors have been investigated for remote health and fitness monitoring, including applications ranging from wound healing to athletic training [8]. Wearable sensors have included ring, ear, and body sensors [8-11]. To power these systems, simple batteries and proximity RF power scavenging [12] have been used. Our approach is to use self-powered biosensors, through sensing and harvesting methods for respiratory effort, and electro-cardiogram (ECG) potentials.

Movements of the chest due to quiet unforced respiration are mostly determined by movements of the rib cage and the abdominal wall. Studies have found that average chest wall displacement due to respiratory effort is on the order of cm [13]. Since respiratory effort itself is a valuable physiological parameter, the method that combines sensing and energy harvesting would enable efficient biosensing.

Our break-through approach is to concurrently harvest and sense physiological signals by reusing the hardware components to perform both functions, managed through a highly efficient control and communication protocol.

3. Preliminary Studies

Our recent work [14-16] to implement self-powered biosensors includes applying a method to detect and harvest respiration signals. However, we do not have a good understanding of how variations in the population affect the performance of our systems, thus we propose the experiments on a large number of subjects for better understanding and improvement of our works.

4. Research Design and Methods

The research experiments consist of measuring and categorizing data from our self-powered wearable biosensor system design. Each experiment will be done in the human performance laboratory located in the Kinesiology Department and is expected to be two one-hour sessions. The list of experimental instruments can be found in Table A.1.

5. Experimental Methods:

5.1 Human Subjects Involvement

Participants for the pilot will be 100 healthy, physically active adults 18 to 85 years of age recruited from the University of Hawaii (UH) student population and the Oahu community. Experimental protocol will include one on-site session. Participants will be instructed to report to the University of Hawaii Human Performance Laboratory in a well-hydrated state. Participants will complete health history and exercise questionnaires and sign the approved informed consent form. A healthcare professional (BOC Certified Athletic Trainer) will review each questionnaire and identify exclusion criteria. The subject's weight, height, and thorax dimensions will be measured. Thorax dimensions will be measured both at full inhale and full exhale – including waist circumference, chest circumference, chest breadth, and chest depth.

Inclusion criteria for all participants includes classification as low risk (ACSM Risk Stratification Categories) for exercise testing and free from any cardiovascular, coronary artery, pulmonary, or metabolic diseases (Mahler DA, Froelicher VF, Miller NH, York TD. ACSM's *Guidelines for Exercise Testing and Prescription*. 7th ed. Baltimore: Lippincott Williams and Wilkins; 2009.). Also being pregnant will exclude the participants from experiment.

Changes to the current protocol do not significantly increase participant risk and qualify as eligible for expedited review since the procedures being added would qualify for expedited review within any new IRB applications.

Participants will be informed of potential risks and that involvement is voluntary. Participants will also be informed they may refuse to participate at any time prior to or during the study without penalty.

5.2 Testing Protocol

Prior to test initiation, participants will be fitted with a heart rate monitor; 2 self-powered wearable respiratory effort sensors (one worn around the chest, and one worn around the stomach), a piezoelectric belt as a chest motion reference, headgear, and breathing mask to assess respiratory gas exchange throughout the test. Participants will breathe through the mask throughout the duration of the test which is connected to a metabolic cart through ventilation tubes. The metabolic cart will be used to determine oxygen consumption (VO2) and respiratory exchange ratio (RER).

Testing conditions will include a range of respiratory effort in order to determine if any effect of biosensor application is consistent across the activity range. Surface EMG electrode placements will be in pairs in the seventh or eighth intercostal space on the right side of the body at the midclavicular line to record the activity of the diaphragm and in the 2nd or 3rd intercostal space at the midclavicular line for the external intercostals muscles.

Testing will begin in the resting condition, followed by assessment during a hyperventilatory condition. The hyperventilatory condition will include forced hyperventilation at a prescribed respiratory rate between 75-100% above resting respiratory rate for a period of less than one minute in each state. Increases in the metabolic cost of the hyperventilatory condition above the resting condition represent the respiratory effort. This condition will be followed by a 10-minute rest before completing the final condition. The final condition will include metabolic and EMG analysis during a submaximal exercise ramp protocol on a cycle ergometer. Subjects will complete 3-minute stages with increasing workloads of 50 Watts per stage until reaching 70% age-predicted-maximum heart rate (=191.5-(0.007*age)). Cycle ergometer testing is expected to last 9-12 minutes for each subject. The headgear and breathing mask will be removed at this time.

Variables of interest between the "control" and "scavenger application" state will include VO2, RER, KCAL expenditure, metabolic efficiency, ratings of perceived exertion (RPE), changes in respiratory muscle activation and indices of breathing economy (e.g. tidal volume, inspiratory time, etc.). For each condition, the control vs. sensor application state will be implemented using a counterbalanced design to determine which state the subject will complete first. Subject testing will include two one-hour sessions. During each session, each subject will be tested in both states for the resting and hyperventilatory condition. The changes between states

will be determined as the average of the 2 sessions. The exercise protocol will be conducted in only one state (control or sensor application) per testing session based on a counterbalanced design.

5.3 Outcome Measures

- Cardiovascular responses will be collected via standard open circuit spirometry. Inspired ventilation was measured with a previously calibrated dry gas meter (Rayfield RAM-9200) fitted with a potentiometer.
- Expired ventilation will be channeled through Hans Rudolf high velocity valve through low resistance plastic tubing into a 5-liter mixing chamber.
- The concentrations of oxygen and carbon dioxide will be continuously sampled with an Applied Electrochemistry Oxygen analyzer S-3A/1, Oxygen sensor N-22M, carbon dioxide analyzer CD-3A, and a carbon dioxide sensor P-61B which will be calibrated with commercially available primary standard grade gases.
- Heart rate will be measured via Model Q710 electrocardiogram (Quinton Instrument Co., Bothell, Washington).
- Respiratory rate and tidal volume will be measured by both spirometry and the self-powered respiratory sensor during all stages.
- Participants will use the 6-20 point Borg Scale (attached) at the end of each stage by pointing to the appropriate RPE value while continuing to exercise.

Table A.1 The experiments consist of the following equipment

Type of Equipment	Equipment Name	Amount
Heart Rate/Respiratory Rate Sensors (incorporated into shirt/belt/upper arm cuff/wrist cuff modules)	Piezoelectric chest belt	1
	Electrocardiogram Quinton Instrument Co Model Q710	1
	Inductive plethysmography sensor	1
	Impedance plethysmography sensor	1
	Resistive elastomers	1
	Photometry sensor	1
	Acoustic (impedance-matched) microphone	1
	Galvanic skin response sensor	**1**
	Customized low voltage rectifier	1
Data Processing and Transmission Module	TI CC430 Wireless link Texas Instruments	1
	6-20 point Borg Scale	1

Type of Equipment	Equipment Name	Amount
RPE reference	Hans Rudolf high velocity valve	1
	Low resistance plastic tubing	1
Velocity Valve	5-liter mixing chamber	1
	Electrochemistry Oxygen analyzer S-3A/1	1
Electrochemistry Oxygen analyzer	Oxygen sensor N-22M	1
	Carbon dioxide analyzer CD-3A	1
Oxygen sensor	Carbon dioxide sensor P-61B	1
Carbon dioxide analyzer	Spirometer	1
Carbon dioxide sensor	Polar wear link chest belt	1
References		

5.4 Risk and hazardous evaluations:

If you have a pacemaker or defibrillator, or have health issues which requires that you wear electronics of any sort, avoid using magnet generators. To be on the safe side we would advise pregnant women to avoid any exposure to magnetic fields. So if you are sexually active you should be in a birth control program in order to be in this study.

6. Data and Safety Monitoring Plan

1. All experiments will be logged.
2. All complaints from the participants will be logged and reported to the PI and CHS.
3. All unanticipated adverse events will be logged and reported to the PI and CHS.

7. Literature Cited

[1] Jansen, A.J.; Stevels, A.L.N., "Human power, a sustainable option for electronics," *Proceedings of the 1999 IEEE International Symposium on Electronics and the Environment*, ISEE 1999.11-13 May 1999 Page(s):215– 218.

[2] J. Kymisis, C. Kendall, J. Paradiso, and N. Gershenfeld, "Parasitic Power Harvesting in Shoes, *Second International Conference on Wearable Computing,* 1998.

[3] L. C. Rome, L. Flynn, E. M. Goldman, and T.D. Yoo, "Generating electricity while walking with loads," *Science*, Vol. 309, Sept. 2005, Page(s): 1725-1728.

[4] C.R. Saha, T. O'Donnell, N.Wang, P. McCloskey, "Electromagnetic generator for harvesting energy from human motion" *Elsevier Sensors and Actuators A: Physical* Vol. 147, Issue 1, 15 Sep. 2008, pp: 248-253.
[5] V. Leonov, T. Torfs, P. Fiorini, and C. Van Hoof, "Thermoelectric Converters of Human Warmth for Self-Powered Wireless Sensor Nodes," *IEEE Sensors Journal*, Vol. 7, No. 5, May 2007.
[6] www.numetrex.com
[7] T. Starner and J. Paradiso, "Human Generated Power for Mobile Electronics," in *Low Power Electronics Design*, CRS Press, Fall 2004.
[8] Morris, Deirdre; Schazmann, Benjamin; Wu, Yangzhe; Coyle, Shirley; Brady, Sarah; Fay, Cormac; Hayes, Jer; Lau, King Tong; Wallace, Gordon; Diamond, Dermot; , "Wearable technology for biochemical analysis of body fluids during exercise," *Engineering in Medicine and Biology Society, EMBS. 30th Annual International Conference of the IEEE* , vol., no., pp.5741-5744, 2025 Aug. 2008.
[9] Asada, H.H.; Shaltis, P.; Reisner, A.; Sokwoo Rhee; Hutchinson, R.C.; , "Mobile monitoring with wearable photoplethysmographic biosensors," *Engineering in Medicine and Biology Magazine, IEEE*, vol.22, no.3, pp. 28- 40, May-June 2003.
[10]Ming-Zher Poh; Swenson, N.C.; Picard, R.W.; , "Motion-Tolerant Magnetic Earring Sensor and Wireless Earpiece for Wearable Photoplethysmography," *Information Technology in Biomedicine, IEEE Transactions on* , vol.14, no.3, pp.786-794, May 2010
[11]J. Yoo, L. Yan, S. Lee, Y. Kim, and H. J. Yoo, "A 5.2 mW Self-Configured Wearable Body Sensor Network Controller and a 12uW Wirelessly Powered Sensor for a Continuous Monitoring System," *IEEE Journal of Solid State Circuits*, Vol. 45, No. 1, January 2010, pp. 178-188.
[12]C.R. Saha, T. O'Donnell, N.Wang, P. McCloskey, "Electromagnetic generator for harvesting energy from human motion" *Elsevier Sensors and Actuators A: Physical* Vol. 147, Issue 1, 15 Sep. 2008, pp: 248-253.
[13]T. Kondo, T. Uhlig, P. Pemberton, P. D. Sly, "Laser monitoring of chest wall displacement," *EurRespir J.* 1997; 10: 1865-9.
[14]O. Boric-Lubecke, V. Lubecke, I. Mostafanezhad, and E. Shahhaidar, "Zero-Net Energy Wearable Biosensors," *ISCA25th International Conference on Computers and Their Applications (CATA- 2010)*, April 2010.
[15]E. Shahhaidar, M. Wolfe, R. Ghorbani, and O. B. Lubecke, "Electromagnetic Generator as Respiratory Effort Energy Harvester," *IEEE Power and Energy Conference*, Urbana-Champaign, Illinois, February 2011.
[16]B. Padasdao, O. B. Lubecke, "Respiratory Rate Detection Using a Wearable Electromagnetic Generator ", *EMBC 2011*.

A.2. CHS #19176 Consent Form

UNIVERSITY OF HAWAI`I

INFORMED CONSENT AND PRIVACY AUTHORIZATION

TO TAKE PART IN A RESEARCH STUDY

Study Title: *Respiratory Effort Sensing and Harvesting*

Principal Investigator (PI):

Name: Dr. Olga Boric-Lubecke

Institutional Affiliation: Electrical Engineering Department, University of Hawaii at Manoa

Address: POST 205K, 1680 East-West Rd Honolulu, HI 96822

Phone Number: (808) 956-9648

Sponsor: REIS

Sponsor Name: Anthony Kuh

Sponsor Address: 2540 Dole Street, Honolulu, Hawaii, 96822

Sponsor: Archinoetics DoD SBIR Phase II subaward

Sponsor Name: Alan Furuno

Sponsor Address: Bldg. 1054 Patchel Street, Fort Detrick, Maryland 21702-5012

Voice: 808-433-3602, E-mail: alan.s.furuno.civ@mail.mil

Abbreviations Used:

UH: University of Hawaii

RA: Research Assistant

BOC: Board of Certification

ECG: Electrocardiogram

EMG: Electromyogram

Before you decide whether or not you would like to take part in this study, you should understand its purpose, how it may help, any risks, and what you will be asked to do. This process is called informed consent. If you agree to take part in the study, you will be asked to sign this consent form.

Before you learn about the study, it is important that you know the following:

- Taking part in this study is completely voluntary.
- If you decide to take part in the study, you can change your mind at any time and withdraw from the study.

What is the purpose of this study?

The objective of this project is to develop and verify self-powered unobtrusive wearable biosensors, in the form of a belt and a shirt, that can sense and harvest energy from breathing and/or heartbeat.

Department of Defense (DoD) is the study sponsor, and the representatives of the DoD will have access to research records as they are the study sponsor.

Why are you being asked to participate in this study?

You are being asked to participate in this study because you are above 18 years old and do not have any significant medical problems.

Researchers plan to enroll a total of 100 participants from Hawaii.

How long will the study take and what procedures will be performed on you?

Each experiment will be done in the human performance laboratory in the Stan Sheriff Center at UH, and is expected to be two sessions, one hour each.

First, participants will undergo the consent process which provides participants time to read the consent form and ask questions. Then, if they agree to participate, participants will sign the consent form.

Next, participants will fill out a health history questionnaire and an exercise questionnaire. The questionnaire will be reviewed by a healthcare professional (BOC certified athletic trainer) to make sure you are healthy enough to participate.

Then the participant's weight, height, and thorax (the part of the human body between the neck and the diaphragm, partially encased by the ribs and containing the heart and lungs; the chest) dimensions will be measured. The thorax dimensions will be measured both at full inhale and full exhale including waist circumference, chest circumference, chest breadth, and chest depth.

Prior to test initiation, participants will be fitted with a heart rate monitor, a sensing module (incorporated into a shirt belt, upper arm cuff, and wrist cuff) comprising heart rate (ECG) and respiratory rate sensors, headgear, and breathing masks to assess respiratory gas exchange throughout the test. Participants will breathe through the mask throughout the duration of the test which is connected to a metabolic cart through ventilation tubes. The metabolic cart will be used to determine oxygen consumption and respiratory exchange ratio.

Testing conditions will include a range of breathing rates in order to determine if any effect of using sensors is observed for all activities. Participants will breathe through the mask throughout the duration of the test to measure parameters of respiration. Surface EMG electrode placements on the chest will be used to monitors muscle movement related to breathing.

Testing will begin in the resting condition, followed by assessment during exercise. The exercise condition will include heavier breathing for a period of less than one minute in each state. This condition will be followed by a 10 minute rest before completing the final condition. The final condition will include walking on an exercise ramp. This testing is expected to last 9-12 minutes for each subject.

What are the risks and discomforts that you may experience?

If you have a pacemaker or defibrillator, or have health issues which require that you wear electronics of any sort, you should not participate in this study.

We would advise pregnant women to not participate in this study. If you are sexually active, you should be in a birth control program if you want to participate in this study.

People who are uncomfortable in confined spaces, have a tendency to be claustrophobic, or who might have a stress reaction to wearing the head gear and mask should not participate in this study.

How will your information be used?

There may not be direct benefit to the participants. However, the results from this project will help better identify and address the issues with respiratory effort sensing and harvesting. Mainly the researchers will look into the differences of the attainable energy from different people of various ages, gender, and physical characteristics.

Representatives of the DoD will have access to research records as they are the study sponsor.

How will my study data be kept confidential?

Research data will be confidential to the extent allowed by law. Agencies with research oversight, such as the UH Human Studies Program, have the authority to review research data. All research records will be stored on a password-protected computer in a locked room in the primary investigator's lab for the duration of the research project, and will be destroyed upon completion of the project.

The results of this research may be presented at meetings or in publications; however, you will not be identified.

Will you be given the results of the study?

The study PI or research assistant will not provide any individual study results to you or any member of your family, other doctors involved in your care, your insurance company, or your employer.

How will this study benefit you?

It is unlikely that you will benefit directly from participating in this study.

Are there costs or payments involved in this study?

There will be no costs or payments for your examination and tests in this study.

Can you revoke your consent for your participation in this study?

If you enter the study and you later change your mind, you can revoke (take away) your consent at any time, and there will be no penalty for you. This means that you can leave the study at any point as you are a voluntary research participant.

The study RA will decide if it is not possible or appropriate for you to continue to participate in this study due to unexpected health concerns or reactions to the experiment. If the study RA observes or believes that you are experiencing significant discomfort or fatigue, and that continuation of the study would be detrimental to your health and safety, your participation in the study will be immediately discontinued.

Will you learn about new findings about risks of this study?

You will be told of any new information learned during the study that may change your willingness to continue in this study. At that time, you will be able to decide whether to continue your participation in this research study.

If you have any questions about this study, whom do you contact?

If you feel that you have been injured as a result of taking part in this study, or if you have any questions about the study, you should call the study PI, [Dr.Olga Boric-Lubecke], at [(808) 956-9648*]*.

If you have questions about your rights as a research participant in this study, you should contact the University of Hawaii Human Studies Program at 808.956.5007 or by email at uhirb@hawaii.edu

Authorization to Use and Disclose (Release) Personal Health Information

The federal government has created a "Privacy Rule" under the Health Insurance Portability and Accountability Act (HIPAA). This Rule gives you the right to decide who can use and release your personal health information (also called "protected health information" or "PHI") for the purposes of research.

PHI is health information about study participants that could be linked to their identity. But we will not use your PHI in this study.

What happens if you do not sign this authorization?

Signing this authorization form is voluntary. If you do not sign this form, you will not take part in this research study.

Consent for You to Take Part in this Research Study

My signature indicates that I have read and understand this research consent/authorization form and that my questions have been satisfactorily answered. I understand that if at any time I have other questions, I can contact the study PI listed on page 1 and page 4 of this form. I further understand that I will be given a copy of this signed consent/authorization form for my records.

_____

Name of the Participant

_____ _____

Signature of the Participant Date

A.3. CHS #19176 Approval Letter

Office of Research Compliance
Human Studies Program

UNIVERSITY of HAWAI'I® MĀNOA

MEMORANDUM
CR

December 2, 2015

TO: Olga Boric-Lubecke, Ph.D.
Principal Investigator
Electrical Engineering

FROM: Denise A. Lin-DeShetler, MPH, MA
Director

SUBJECT: CHS #19176- "A Pilot Study for Respiratory Effort Sensing and Harvesting"

Under an expedited review procedure, the research project identified above was approved for one year on November 27, 2015 by the University of Hawaii (UH) Human Studies Program. The application qualified for expedited review under CFR 46.110 and 21 CFR 56.110, Category (7).

This memorandum is your record of the Human Studies Program approval of this study. Please maintain it with your study records.

The Human Studies Program approval for this project will expire on November 26, 2016. If you expect your project to continue beyond this date, you must submit an application for renewal of this Human Studies Program approval. The Human Studies Program approval must be maintained for the entire term of your project.

If, during the course of your project, you intend to make changes to this study, you must obtain approval from the Human Studies Program prior to implementing any changes. If an Unanticipated Problem occurs during the course of the study, you must notify the Human Studies Program within 24 hours of knowledge of the problem. A formal report must be submitted to the Human Studies Program within 10 days. The definition of "Unanticipated Problem" may be found at: http://hawaii.edu/irb/download/documents/SOPP_101_UP_Reporting.pdf, and the report form may be downloaded here: http://hawaii.edu/irb/download/forms/App_UP_Report.doc.

You are required to maintain complete records pertaining to the use of humans as participants in your research. This includes all information or materials conveyed to and received from participants as well as signed consent forms, data, analyses, and results. These records must be maintained for at least three years following project completion or termination, and they are subject to inspection and review by the Human Studies Program and other authorized agencies.

1960 East-West Road
Biomedical Sciences Building B104
Honolulu, Hawai'i 96822
Telephone: (808) 956-5007
Fax: (808) 956-8683

References

[1] K.D. Kochanek, et al. National Vital Statistics Reports - Deaths: Final Data for 2014.NVSS, vol. 65, no. 4, June 2016.

[2] A. Droitcour, "Non-contact measurement of heart and respiration rates with a single-chip microwave Doppler Radar," Ph.D. dissertation, Dept. of Electrical Engineering, Stanford University, Stanford, CA, 2006.

[3] Starner, Thad. "Human-powered wearable computing." *IBM systems Journal*, 35, no. 3.4 (1996): 618-629.

[4] De Pasquale, Giorgio, and A. Somà. "Energy harvesting from human motion with piezo fibers for the body monitoring by MEMS sensors." *Design, Test, Integration and Packaging of MEMS/MOEMS (DTIP), 2013 Symposium on*. IEEE, 2013.

[5] Mhetre, Manisha R., and H. K. Abhyankar. "Voltage generation using piezoelectric sensor from Human exhalation." *Computing for Sustainable Global Development (INDIACom), 2015 2nd International Conference on. IEEE*, 2015.

[6] S. Rajala and J. Lekkala, "Film-Type Sensor Materials PVDF and EMFi in Measurement of Cardiorespiratory Signals - A Review", *IEEE Sensors Journal*, vol. 12, no. 3, pp. 439-446, 2012.

[7] Kobayashi, Makiko, Takahiko Ikari, Shugo Kurose, and Tomohiko Igasaki. "Heartbeat interval monitoring by PZT/PZT flexible piezoelectric film sensor." In *Ultrasonics Symposium (IUS), 2015 IEEE International*, pp. 1-3. IEEE, 2015.

[8] Buxi, Dilpreet, Jean-Michel Redouté, and Mehmet Rasit Yuce. "A frequency-sensing readout using piezoelectric sensors for sensing of physiological signals." *2014 36th Annual International Conference of the IEEE Engineering in Medicine and Biology Society*, 2014.

[9] Klap, Tal, and Zvika Shinar. "Using piezoelectric sensor for continuous-contact-free monitoring of heart and respiration rates in real-life hospital settings." *Computing in Cardiology 2013. IEEE*, 2013.

[10] Toshiyo Tamura, Yuka Maeda, Masaki Sekine and Masaki Yoshida, "Review: Wearable Photoplethysmographic Sensors—Past and Present," *Electronics*, 2014, 3(2), 282-302; doi:10.3390/electronics3020282.

[11] Suzuki, Takuji, Ken-ichi Kameyama, and Toshiyo Tamura. "Development of the irregular pulse detection method in daily life using wearable photoplethysmographic sensor." In *2009 Annual International Conference of the IEEE Engineering in Medicine and Biology Society*, pp. 6080-6083. IEEE, 2009.

[12] Lee, Y.; Shin, H.; Jo, J.; Lee, Y. Development of a wristwatch-type PPG array sensor module. In *Proceedings of the IEEE International Conference on Consumer Electronics*, Berlin, Germany, 6–8 September 2011; pp. 168–171.

[13] Lee, SeungMin, HyunSoon Shin, and ChanYoung Hahm. "Effective PPG sensor placement for reflected red and green light, and infrared wristband-type photoplethysmography." In *2016 18th International Conference on Advanced Communication Technology (ICACT)*, pp. 556-558. IEEE, 2016.

[14] Lee, Boon-Giin, Boon-Leng Lee, and Wan-Young Chung. "Smartwatch-based driver alertness monitoring with wearable motion and physiological sensor." In *2015 37th Annual International Conference of the IEEE Engineering in Medicine and Biology Society (EMBC)*, pp. 6126-6129. IEEE, 2015.

[15] Maguire, Michael, and Tomas Ward. "The design and clinical use of a reflective brachial photoplethysmograph." (2002).

[16] Maeda, Yuka, Masaki Sekine, and Toshiyo Tamura. "Relationship between measurement site and motion artifacts in wearable reflected photoplethysmography." *Journal of medical systems* 35, no. 5 (2011): 969-976.

[17] Patterson, James AC, Douglas C. McIlwraith, and Guang-Zhong Yang. "A flexible, low noise reflective PPG sensor platform for ear-worn heart rate monitoring." In *2009 Sixth International Workshop on Wearable and Implantable Body Sensor Networks*, pp. 286-291. IEEE, 2009.

[18] Vogel, Stefan, Markus Hülsbusch, Thomas Hennig, Vladimir Blazek, and Steffen Leonhardt. "In-ear vital signs monitoring using a novel microoptic reflective sensor." *IEEE Transactions on Information Technology in Biomedicine* 13, no. 6 (2009): 882-889.

[19] Cha, Ji-Young, Hyun-Seok Choi, Jae-Yeon Shin, and Kyoung-Joung Lee. "Unconstrained respiration and heart rate monitoring system based on a PPG pillow during sleep." In *2008 30th Annual International Conference of the IEEE Engineering in Medicine and Biology Society*, pp. 3224-3226. IEEE, 2008.

[20] Kim, Sang Hyun, Dong Wan Ryoo, and Changseok Bae. "U-healthcare system using smart headband." In *2008 30th Annual International Conference of the IEEE Engineering in Medicine and Biology Society*, pp. 1557-1560. IEEE, 2008.

[21] B. S. Kim and S. K. Yoo, "Motion artifact reduction in photoplethysmography using independent component analysis," *IEEE Trans. Biomed. Eng.*, vol. 53, no. 3, pp. 566–568, Mar. 2006.

[22] M. R. Ram, K. V. Madhav, E. H. Krishna, N. R. Komalla, and K. A. Reddy, "A novel approach for motion artifact reduction in PPG signals based on AS-LMS adaptive filter," *IEEE Trans. Instrum. Meas.*, vol. 61, no. 5, pp. 1445–1457, May 2012.

[23] H. Han and J. Kim, "Artifacts in wearable photoplethysmographs during daily life motions and their reduction with least mean square based active noise cancellation method," *Comput. Biol. Med.*, vol. 42, no. 4, pp. 387–393, Apr. 2012.

[24] Z. Zhang, Z. Pi, and B. Liu, "TROIKA: A general framework for heart rate monitoring using wrist-type photoplethysmographic signals during intensive physical exercise," *IEEE Trans. Biomed. Eng.*, vol. 62, no. 2, pp. 522–531, Feb. 2015.

[25] Y. Zhang, B. Liu, and Z. Zhang, "Combining ensemble empirical mode decomposition with spectrum subtraction technique for heart rate monitoring using wrist-type photoplethysmography," *Biomed. Signal Process. Control*, vol. 21, pp. 119–125, Aug. 2015.

[26] Gonzalez-Landaeta, Rafael, Oscar Casas, and Ramon Pallas-Areny. "Heart rate detection from plantar bioimpedance measurements." *IEEE Transactions on Biomedical Engineering* 55, no. 3 (2008): 1163-1167.

[27] L. Nescolarde, J. Yanguas, et al, "Assessment and follow-up of muscle injuries in athletes by bioimpedance: Preliminary results," *IEEE 33rd Annual International Conference of the EMBS*, Boston, Massachusetts, USA, Aug. 30 - Sept. 3, 2011

[28] Fritz Mellert, Kai Winkler, et al, "Detection of (Reversible) Myocardial Ischemic Injury by Means of Electrical Bioimpedance," *IEEE Transactions on Biomedical Engineering*, vol.58, no. 6, June 2011

[29] A. R. Al-Hashimi, A. N. Nordin, and A. W. Azman, "Bioimpedance spectroscopy system for Characterization of Cancer Cells," *5th International Conference on Intelligent and Advanced Systems (ICIAS)*, Kuala Lumpur, June 2014

[30] S. M. M. Naidu, Uttam R. Bagal, Prem C. Pandey, et al, "Monitoring of Stroke Volume through Impedance Cardiography Using an Artificial Neural Network", *21st National Conference on Communications (NCC)*, Mumbai, Feb. 27 - March 1, 2015

[31] Ji-Jer Huang, Yang-Min Huang, Ming-Wen Chang, "Using bioimpedance plethysmography for measuring the pulse wave velocity of peripheral vascular," *Electrical Engineering/Electronics, Computer, Telecommunications and Information Technology (ECTI-CON), 2016 13th International Conference on*, June 28 - July 1, 2016.

[32] Buxi, Dilpreet, Jean-Michel Redoute, and Mehmet Rasit Yuce. "Blood Pressure Estimation using Pulse Transit Time from Bioimpedance and Continuous Wave Radar." *IEEE Transactions on Biomedical Engineering*, 20 June 2016.

[33] Padma Batra1 and Rajiv Kapoor, "A Novel Method For Heart Rate Measurement Using Bioimpedance," *International Conference on Advances in Recent Technologies in Communication and Computing*, Kottayam, 16-17 Oct. 2010

[34] Delia H. Diaz, Ó Casas, and Ramon Pallas-Areny, ”Heart Rate Detection from Single-Foot Plantar Bioimpedance Measurements in a Weighing Scale”, *IEEE 32nd Annual International Conference of the EMBS*, Buenos Aires, Argentina, August 31 - September 4, 2010

[35] M.-C. Cho, J.-Y. Kim, and S. Cho. “A bio-impedance measurement system for portable monitoring of heart rate and pulse wave velocity using small body area,” *IEEE International Symposium on Circuits and Systems (ISCAS)*, pp. 3106-3109, 24-27 May, 2009

[36] Droitcour, Amy D., Olga Boric-Lubecke, Victor M. Lubecke, Jenshan Lin, and Gregory TA Kovacs. "Range correlation and I/Q performance benefits in single-chip silicon Doppler radars for noncontact cardiopulmonary monitoring." *IEEE Transactions on Microwave Theory and Techniques* 52, no. 3 (2004): 838-848.

[37] Xiao, Yanming, Jenshan Lin, Olga Boric-Lubecke, and M. Lubecke. "Frequency-tuning technique for remote detection of heartbeat and respiration using low-power double-sideband transmission in the Ka-band." *IEEE Transactions on Microwave Theory and Techniques* 54, no. 5 (2006): 2023-2032.

[38] Gu, Changzhan, Ruijiang Li, Hualiang Zhang, Albert YC Fung, Carlos Torres, Steve B. Jiang, and Changzhi Li. "Accurate respiration measurement using DC-coupled continuous-wave radar sensor for motion-adaptive cancer radiotherapy." *IEEE Transactions on Biomedical Engineering* 59, no. 11 (2012): 3117-3123.

[39] Wang, Guochao, José-María Muñoz-Ferreras, Changzhan Gu, Changzhi Li, and Roberto Gómez-García. "Application of linear-frequency-modulated continuous-wave (LFMCW) radars for tracking of vital signs." *IEEE Transactions on Microwave Theory and Techniques* 62, no. 6 (2014): 1387-1399.

[40] Wang, Siying, Antje Pohl, Timo Jaeschke, Michael Czaplik, Marcus Köny, Steffen Leonhardt, and Nils Pohl. "A novel ultra-wideband 80 GHz FMCW radar system for contactless monitoring of vital signs." In *37th Annual International Conference of the IEEE Engineering in Medicine and Biology Society (EMBC)*, pp. 4978-4981. IEEE, 2015.

[41] Baboli, Mehran, Olga Boric-Lubecke, and Victor Lubecke. "Heart and respiratory detection and simulations for tracking humans based on respiration by using pulse-based radar." In *NORCHIP*, pp. 1-4. IEEE, 2012.

[42] Wang, Yazhou, Quanhua Liu, and Aly E. Fathy. "Simultaneous localization and respiration detection of multiple people using low cost UWB biometric pulse Doppler radar sensor." In Microwave Symposium Digest (MTT), *2012 IEEE MTT-S International*, pp. 1-3., 2012.

[43] Y.E. Moskalenko, “On the Application of Centimeter Radio Waves for Electrodeless recordings of volume changes of biological objects,” *Biophysics (USSR)*, vol. 5, pp. 225-228, 1960

[44] Massagram, Wansuree, Noah Hafner, Victor Lubecke, and Olga Boric-Lubecke. "Tidal volume measurement through non-contact Doppler radar with DC reconstruction." *IEEE Sensors Journal* 13, no. 9 (2013): 3397-3404.

[45] W. Massagram, V.M. Lubecke, A. Host-Madsen and O. Boric-Lubecke, "Assessment of Heart Rate Variability and Respiratory Sinus Arrhythmia via Doppler Radar," *IEEE Trans. Microw. Theory Techn.*, vol. 57, no. 10, pp. 2542-2549, Oct 2009

[46] J.Y. Lee, J.C. Lin, "A Microcprocessor-Based Noninvasive Arterial Pulse Wave Analyzer," *IEEE Trans. Biomed. Eng.*, vol. BME-32, no. 6, pp. 451-455, June 1985.

[47] L. Li, C. Li and D.Y.C. Lie, "Experimental Demonstration of Noncontact Pulse Wave Velocity Monitoring Using Multiple Doppler Radar Sensors," in *IEEE EMBC*, Buenos Aires, 2010, pp. 5010-5013

[48] Tao, Teh-Ho, Shin-Jen Hu, Jla-Hung Peng, and Su-Chen Kuo. "An ultrawideband radar based pulse sensor for arterial stiffness measurement." In *2007 29th Annual International Conference of the IEEE Engineering in Medicine and Biology Society*, pp. 1679-1682. IEEE, 2007.

[49] Soh, Ping Jack, Marco Mercuri, Gokarna Pandey, Guy AE Vandenbosch, and Dominique MM-P. Schreurs. "Dual-band planar bowtie monopole for a fall-detection radar and telemetry system." *IEEE Antennas and Wireless Propagation Letters* 11 (2012): 1698-1701.

[50] Lee, Yee Siong, Pubudu N. Pathirana, Christopher Louis Steinfort, and Terry Caelli. "Monitoring and analysis of respiratory patterns using microwave doppler radar." *IEEE journal of translational engineering in health and medicine* 2 (2014): 1-12.

[51] Zakrzewski, Mari, Antti Vehkaoja, Atte S. Joutsen, Karri T. Palovuori, and Jukka J. Vanhala. "Noncontact Respiration Monitoring During Sleep With Microwave Doppler Radar." *IEEE Sensors Journal* 15, no. 10 (2015): 5683-5693.

[52] Yavari, Ehsan, Chenyan Song, Victor Lubecke, and Olga Boric-Lubecke. "System-on-Chip based Doppler radar occupancy sensor." In *2011 Annual International Conference of the IEEE Engineering in Medicine and Biology Society*, pp. 1913-1916. IEEE, 2011.

[53] E. Yavari, H. Jou, V. Lubecke, and O. Boric-Lubecke, "Doppler radar sensor for occupancy monitoring," in *Proc. 2013 IEEE Radio Wireless Symp.*, pp. 316–318.

[54] Changzhan Gu and Changzhi Li, "From Tumor Targeting to Speech Monitoring: Accurate Respiratory Monitoring Using Medical Continuous-Wave Radar Sensors", *Microwave Magazine IEEE*, vol. 15, pp. 66-76, 2014, ISSN 1527-3342.

[55] V. M. Lubecke, O. Boric-Lubecke, A. Host-Madsen, and A. E. Fathy, "Through-the-wall radar life detection and monitoring," in *Proc. IEEE/MTT-S Int. Microwave Symp.*, June 2007, pp. 769–772.

[56] P. H. Chen and R. M. Narayanan, "Shifted pixel method for through-wall radar imaging," *IEEE Trans. Antennas Propagat.*, vol. 60, no. 8, pp. 3706–3716, 2012.

[57] W. Yazhou and A. E. Fathy, "Advanced system level simulation platform for three-dimensional UWB through-wall imaging SAR using time-domain approach," *IEEE Trans. Geosci. Remote Sensing*, vol. 50, no. 5, pp. 1986–2000, 2012.

[58] Fear, E. G., and J. M. Sill. "Preliminary investigations of tissue sensing adaptive radar for breast tumor detection." In *Engineering in Medicine and Biology Society, 2003. Proceedings of the 25th Annual International Conference of the IEEE*, vol. 4, pp. 3787-3790. IEEE, 2003.

[59] E. C. Fear, J. Bourqui, C. Curtis, D. Mew, B. Docktor, and C. Romano, "Microwave breast imaging with a monostatic radarbased system: A study of application to patients," *IEEE Trans. Microwave Theory Tech.*, vol. 61, no. 5, pp. 1–10, 2013.

[60] B. Matteo, M. Caruso, M. S. Khan, A. Bevilacqua, A.-D. Capobianco, and A. Neviani, "An integrated microwave imaging radar with planar antennas for breast cancer detection," *IEEE Trans. Microwave Theory Tech.*, vol. 61, no. 5, pp. 1–11, 2013.

[61] Mohd Azlishah Othman, Mohan Sinnappa, Hazwani Azman, et al, "5.8 GHz Microwave Doppler Radar for Heartbeat Detection," *23rd Int'l Conf. on Radioelectronika*, Pardubice, Czech Republic, 2013, pp. 367-370.

[62] O. Boric-Lubecke, P.-W. Ong, and V. M. Lubecke, "10 GHz Doppler Radar Sensing of Respiration and Heart Movement," in Proc. *IEEE 28th Annual Northeast Bioengineering Conference*, Philadelphia, 2002, pp. 55-56.

[63] D.Obeid, S.Sadek, G. Zaharia, and G. El Zein, "A Tunable System for Contact-less Heartbeat Detection and a Modeling Approach," *Medical Applications Networking (MAN), IEEE ICC*, 2009, pp. 1-5.

[64] Ramin Fadaei Fouladi and Ahmet Oncu, "Vital Signs Modeling For Doppler Radar Cardiorespiratory Monitoring," *36th International Conference on Telecommunications and Signal Processing (TSP)*, Rome, 2013, pp. 363-366.

[65] Wei Hu, Zhangyan Zhao, Yunfeng Wang, and Haiying Hui, "Noncontact Accurate Measurement of Cardiopulmonary Activity Using a Compact Quadrature Doppler Radar Sensor," *IEEE Trans. Biomedical Engineering*, vol. 61, no. 3, pp. 725-735, Mar. 2014.

[66] Øyvind Aardal, Svein-Erik Hamran, Tor Berger, "Chest Movement Estimation from Radar Modulation Caused by Heartbeats," *2011 IEEE Biomedical Circuits and System Conference*, San Diego, pp. 452-455.

[67] Changzhi Li, and Jenshan Lin, "Non-Contact Measurement of Periodic Movements by a 22-40GHz Radar Sensor Using Nonlinear Phase Modulation," *IEEE MTT-S International Microwave Symposium*, Honolulu, 2007, pp. 579-582.

[68] J.E. Kiriazi, “Human Cardiopulmonary Recognition Using Close-range Doppler Radar,” Ph.D. dissertation, Dept. Elect. Eng., Univ. of Hawaii, Honolulu, HI, 2010.

[69] B.-K. Park, A. Vergara, O. Boric-Lubecke, V. Lubecke, and A. Høst-Madsen, “Quadrature demodulation with DC cancellation for a Doppler radar motion detector,” *unpublished. Available: http://www.ee.hawaii.edu/~madsen/papers/.*

[70] M. Zakrzewski, H. Raittinen, et al, “Comparison of Center Estimation Algorithms for Heart and Respiration Monitoring with Microwave Doppler Radar,” *IEEE Sensors J.*, vol. 12, no. 3, pp. 627-634, Mar. 2012.

[71] Okumura, S., T. Sakamoto, T. Sato, M. Yoshioka, K. Inoue, T. Fukuda, and H. Sakai. "Comparison of clutter rejection techniques for measurement of small displacements of body surface using radar." *Electronics Letters*(2016).

[72] Xiaomeng Gao, Aditya Singh, Ehsan Yavari, et al, “Non-contact Displacement Estimation Using Doppler Radar,” *34th Annual International Conference of the IEEE EMBS*, San Diego, 2012, pp. 1602-1605.

[73] T. M. R. Shankar, J. G. Webster, and S.-Y. Shao, “The Contribution of Vessel Volume Change and Blood Resistivity Change to the Electrical Impedance Pulse”, *IEEE Transaction on Biomedical Engineering*, vol. 32, no. 3, March 1985

[74] M.-C. Cho, J.-Y. Kim, and S. Cho. “A bio-impedance measurement system for portable monitoring of heart rate and pulse wave velocity using small body area,” *IEEE International Symposium on Circuits and Systems (ISCAS)*, pp. 3106-3109, 24-27 May, 2009.

[75] J. G. Webster, Medical Instrumentation: Application and Design, *Wiley & Sons*, 3rd ed., 1997

[76] Merrill, I. Skolnik. "Introduction to radar systems." *Mc Graw-Hill*, 1962.

[77] W. Massagram, “A Study of Feasibility in Long-term Cardiopulmonary Monitoring via Doppler Radar,” Ph.D. dissertation, Dept. Elect. Eng., Univ. of Hawaii, Honolulu, HI, 2008.

[78] S. Yamada, O. Boric-Lubecke, and V.M. Lubecke, “Cancellation techniques for LO leakage and DC offset in direct conversion systems,” In *IEEE MTT-S International Microwave Symposium Digest*, pp. 1191-1194, June 2008.

[79] B.-K. Park, O. Boric-Lubecke, V. Lubecke, “Arctangent Demodulation with DC Offset Compensation in Quadrature Doppler Radar Receiver Systems,” *IEEE Trans. Microw. Theory Techn.*, vol. 55, no. 5, pp. 1073-1079, May. 2007.